ACS Catalysis

Open Access

pubs.acs.org/acscatalysis

Research Article

Interplay of Acid Sites and Surface Hydrophobicity in Tin Silicate Catalysts

Lucie Leonova, Zdenek Moravec, Petr Sazama, Tomas Pokorny, Dalibor Kaucky, Areej Fatima, Tomas Homola, Damien P. Debecker,* and Ales Styskalik*

Cite This: *ACS Catal.* 2026, 16, 8199–8217

Read Online

ACCESS | Metrics & More | Article Recommendations | Supporting Information

ABSTRACT: Tin-containing silicates are ubiquitous heterogeneous catalysts for biomass conversion and fine chemicals synthesis, owing to their strong and selective Lewis acidity. Traditionally, these materials are synthesized via multistep procedures such as dealumination of zeolites followed by tin incorporation, which usually offer only limited control over texture and poor metal dispersion. The nonhydrolytic sol-gel (NHSG) method offers a streamlined alternative for synthesizing metal silicates with enhanced control over composition, porosity, and active site dispersion. Here, we employed three NHSG routes, i.e., alkyl halide elimination, acetamide elimination, and their combination, to prepare porous tin silicates. Remarkably, the combined route yielded catalysts with high specific surface areas (up to 900 m^2 g^{-1}, without requiring the use of any pore-generating agent), uniform tin dispersion, and high Lewis acidity. This correlated with comparable activity in dihydroxyacetone (DHA) conversion to ethyl lactate and aminolysis of styrene oxide to reported literature. Modification with trimethylsilyl groups was used to further tune the catalytic behavior by modulating surface polarity. While hydrophobization markedly improved apparent turnover frequencies—up to fivefold in styrene oxide aminolysis—excessive silylation was detrimental to DHA conversion, underscoring the dual role of Si−OH and Si−$OSiMe_3$ groups in catalytic performance.

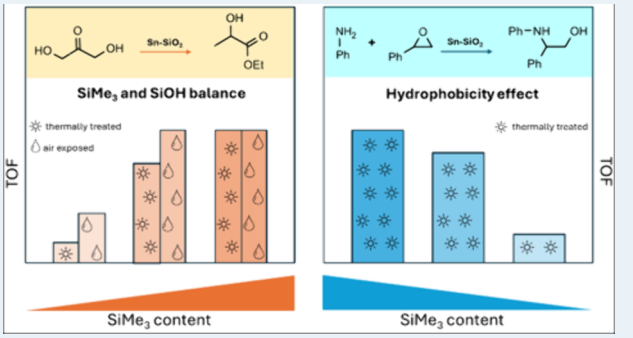

KEYWORDS: *nonhydrolytic sol-gel, tin silicate, surface modification, ethyl lactate, epoxide ring opening, open acid sites, silanol groups*

1. INTRODUCTION

Among solid catalysts, amorphous tin silicates or crystalline tin zeolites have emerged as versatile materials capable of driving various transformations, including selective oxidation,[1−3] dehydrogenation,[4,5] and isomerization of sugars.[6−9] Their catalytic efficiency is largely dictated by the nature of their acid sites derived from tin centers embedded in the silicate framework. Understanding how synthetic strategy influences tin incorporation, acidity, and catalytic behavior is essential for the optimization of their performance during catalytic reactions.[10,11]

Tin silicates are known to feature some Brønsted acidity.[12−14] These acid sites are usually weak and associated with defects in the structure, i.e., SiOH groups in close proximity to the tin sites. However, the presence of Brønsted acid sites in tin silicates is rare, instead it is likely brought by other elements, like retaining Al^{III} during partial zeolite dealumination[15] or introduction of carbon bearing functional acid groups.[16] The genuine catalytic sites mainly arise from well-inserted 4-coordinated and thus coordinatively unsaturated tin atoms acting as Lewis acid sites (LAS). They may be present as tetrahedrally coordinated, nonhydrolyzed SnO_4 units ("closed" Lewis acid sites), in which Sn is fully incorporated into the silicate framework. They can also appear as partially hydrolyzed $HOSnO_3$ species ("open" Lewis acid sites) associated with local framework defects generated through hydrolysis. In addition, isolated $HOSiO_3$ silanol groups may coexist near Sn sites, contributing to the defect environment.[17,18] Small tin clusters or extraframework species in the form of separated tin(IV) oxide phases can be created, when tin is not well-incorporated in the silicate network.[19]

Acid sites of different nature have different catalytic activity. Small SnO_x clusters can be catalytically active e.g. in Bayer-Villiger-oxidation (BVO).[20] However, the higher impact on catalytic activity in BVO is embodied by the LAS amount,[21,22] more specifically catalytic activity was ascribed to partially hydrolysed $HOSnO_3$.[23] Similarly, open $HOSnO_3$ sites facilitate the initial deprotonation during Meerwein−Ponndorf−Verley (MPV) reactions.[24] Furthermore, density functional theory

Received: January 12, 2026
Revised: April 3, 2026
Accepted: April 3, 2026
Published: April 21, 2026

https://doi.org/10.1021/acscatal.6c00144
ACS Catal. 2026, 16, 8199–8217

(DFT) calculations revealed that tin silicates possessing open sites enhance isomerization more efficiently than closed $Sn(OSi)_4$ sites.[25] The reaction proceeds in a more energetically favorable manner due to the stabilization of the transition state by hydrogen bonding between an intermediate and Sn−OH. In contrast, Li et al. argued that the higher the total Lewis acidity (both open and closed acid sites), the higher the selectivity to alkyl lactate produced from triose and the higher the alkyl lactate yield.[12]

Besides acid sites, the catalytic activity can be significantly influenced by the material's hydrophobic degree. In Sn-Beta zeolites, the confinement of Lewis acidic Sn centers within microporous environments with varying defect densities and thus hydrophobicity directly affects the distribution and stability of reactive and inhibitory dimeric intermediates during ethanol dehydration.[26] Hydrophobic environments also regulate the structure of confined hydrogen-bonding solvent networks, which alters adsorption and transition state energetics during catalysis. Consequently, it results in higher activity over hydrophobic Sn-Beta zeolite during MPV reaction compared to the hydrophilic analogue.[27] Similarly, hydrophobized Sn zeolites were also more active in the BVO reaction.[28] The hydrophobicity role in catalytic activity was also elucidated in tin silicates decorated with methyl groups during alkyl lactate production from triose.[29] Post-synthetic treatment of nano-Sn-Beta zeolites with fluoride resulting in low defect hydrophobic Sn zeolites led to a higher catalytic activity in epoxide ring opening by alcohol.[30]

Arguably, (hybrid) tin silicates have the potential to facilitate reactions that produce important chemicals and intermediates. However, a proper tin insertion into the siliceous structure may be challenging due to an immense difference between the tin and silicon ionic radii (0.71 Å for Sn^{4+} and 0.41 Å for Si^{4+}) and low stability of tetrahedrally coordinated Sn atoms. Synthetic strategies for tin silicates vary in the literature and new approaches have been explored, including solid-gas reaction,[2] solid state insertion[31]/ exchange,[32] electro-assisted synthesis,[33] hydrothermal sol-gel,[34] aerosol-assisted sol-gel,[35] thermal degradation of tin(IV) siloxane,[36] and synthesis under water-free conditions.[37−39] Post-synthetic zeolite treatment with $SnCl_4$ (solid-gas reaction) at 500 °C can embed up to 5.9 wt % Sn while releasing less than 3% of Si. Up to 5 wt % Sn can be isomorphically substituted in β-zeolite via solid state incorporation.[31] On the other hand, the electro-assisted method allows a synthesis of tin rich Sn-Beta zeolites with 12 wt %.[33]

However, Sn-doped zeolites are usually microporous leading to limited application in catalysis due to diffusional restriction. Mesoporous tin silicates may offer an alternative, but the tin insertion into the silicate matrices can be complicated. For example, hydrothermal synthesis was shown to yield mesoporous tin silicates composed of separated SnO_2 and SiO_2 phases.[34] Other mesoporous tin silicates prepared by precursors self-assembly combined with hydrothermal sol-gel synthesis resulted in moderately ordered materials.[4] Promisingly, an aerosol-assisted sol-gel route led to a templated synthesis of mesoporous tin silicates with well-inserted tin atoms offering an alternative to hydrothermal synthesis. The water-free synthesis between tetraethylorthosilicate (TEOS) and tin(IV) acetate in anhydrous acetic acid also provided mesoporous $(Si,Sn)O_2$ gels.[37] Another anhydrous approach, so-called twin polymerization, led to formation of SnO_2 particles embedded in SiO_2 polymers.[39] Similarly, NHSG polycondensation of silicon tetraacetate and tetrakis(diethylamido)tin in molar ratio of 1:1 provided well-dispersed SnO_2 nanoparticles in mesoporous silica.[38]

Over the last decades, the NHSG method has been explored for the preparation of various (hybrid) mixed metal porous oxides. Importantly, resulting materials have already been successfully applied as heterogeneous catalysts in ethanol dehydration,[40] ethanol to butadiene transformation,[41] volatile organic compound oxidation,[42] epoxide ring opening,[38,43,44] alkene epoxidation,[45] or olefin metathesis.[46] Their excellent catalytic activity results from good textural properties and homogeneously distributed metal centers in a silicate structure. However, in the particular case of tin silicates mentioned above,[38] the tin sites could not be truly isolated in silica, as the Si:Sn molar ratio applied in the synthesis was 1.

This work explores the tin silicate synthesis using various nonhydrolytic condensation pathways, including alkyl halide elimination, acetamide elimination, and their combination. The first objective was to identify the most suitable type of NHSG condensation for tin silicate synthesis with a special focus on tin dispersion and porosity. Second, post-synthetic grafting of NHSG-prepared tin silicates with hydrophobic trimethylsilyl groups was studied. Hence, the hydrophobization impact on catalytic performance is evaluated in two reactions: (i) epoxide ring opening that benefits from a hydrophobic environment and (ii) ethyl lactate (EL) production via the reaction of dihydroxyacetone (DHA) with ethanol that produces water as a byproduct. This study provides insights into the relationship between tin incorporation (and thus Lewis acidity), surface properties (thus hydrophobicity), and catalytic activity in two unrelated catalytic reactions.

2. EXPERIMENTAL SECTION

General experimental methods, characterization techniques, and spectroscopic characterization data can be found in the Supporting Information.

Catalyst Synthesis:

Synthesis of Inorganic Tin Silicate by Acetamide Elimination. In the autoclave placed in a dry box, $Si(OAc)_4$ (8.549 g, 32.35 mmol) was dissolved in dichloromethane (30 cm^3), and silylated Pluronic F127 (2.995 g, silylation procedure described in the Supporting Information) was added. After dissolving, $Sn(NEt_2)_4$ (0.1819 g, 0.4467 mmol) dissolved in toluene (10 cm^3) was subsequently added to the autoclave. The autoclave was sealed and kept in an oven at 180 °C for 168 h, for gelation. Volatiles and byproducts were distilled under vacuum at 90 °C overnight. The template and residual organic groups were removed by calcination in flowing air at 500 °C (5 °C min^{-1}) for 5 h. The final white product was labeled as **SiSn-Ac**, standing for tin silicate prepared by acetamide elimination.

Synthesis of Inorganic Tin Silicate by Alkyl Halide Elimination. In the autoclave placed in a dry box, $SiCl_4$ (5.46 g, 32.14 mmol) dissolved in dichloromethane (40 cm^3) was mixed with diisopropyl ether (6.665 g, 65.23 mmol) and $SnCl_4$ (0.11 g, 0.422 mmol). The sealed autoclave was placed in an oven at 110 °C for 168 h. After cooling and opening the autoclave in the glove box, a sol was formed. Thus, the autoclave was sealed again and kept in the oven for additional 72 h at 145 °C. The formed gel was transferred into a Schlenk vessel in the dry box and dried under vacuum at 90 °C overnight. Solvent and volatile by products were removed and analyzed via gas chromatography coupled with mass spectrometry (GC-MS). The final white product was recovered by calcination in flowing air at 500 °C (5 °C min^{-1}) for 5 h. It is referred to as **SiSn-RCl**, indicating tin silicate synthesized by alkyl halide elimination.

Synthesis of Inorganic Tin Silicate by Alkyl Halide Elimination Combined with Delayed Acetamide Elimination. In the autoclave placed in a dry box, $SiCl_4$ (5.171 g, 30.44 mmol) was dissolved in dichloromethane (20 cm^3). Diisopropyl ether (5.453 g, 53.37 mmol) and

https://doi.org/10.1021/acscatal.6c00144
ACS Catal. 2026, 16, 8199−8217

$SnCl_4$ (0.014 g, 0.0537 mmol) were directly added to the solution. The autoclave was sealed and placed in an oven at 145 °C for 20 h. After cooling down, the autoclave was opened again in the dry box, a sol was formed. Then, $Si(OAc)_4$ (1.149 g, 4.35 mmol) dissolved in dichloromethane (10 cm^3), and $Sn(NEt_2)_4$ (0.1727 g, 0.42 mmol) dissolved in toluene (10 cm^3) were added into the reaction mixture in the autoclave. The sealed autoclave was kept in an oven at 180 °C for 148 h. During that time, gelation occurred. Afterward, the gel was transferred into a Schlenk vessel and dried under vacuum at 90 °C overnight. The separated volatile liquid phase was analyzed via GC-MS. Calcination was performed in flowing air at 500 °C (5 °C min^{-1}) for 5 h. The resulting white powder was marked as **SiSn-RCl+Ac** signifying synthesis via alkyl halide elimination combined with delayed acetamide elimination. The practical yield of calcined product approaches 100%.

A new batch of the sample **SiSn-RCl+Ac** was prepared by alkyl halide elimination combined with a delayed acetamide elimination route to ensure sufficient amount of tin silicate matrix for modification (labeled as **SiSn-parent** in the following part). Precursors amounts, solvent volumes, and **SiSn-parent** yield are detailed in the Supporting Information. Characterization of **SiSn-parent** (N_2 porosimetry, XPS, etc.) showed reproducible results with respect to **SiSn-RCl+Ac** (Supporting Information).

Tin Silicate Modification

The **SiSn-parent** degassed overnight either at room temperature or 500 °C under vacuum (~10^{-3} Torr) was dispersed in dry toluene (10 cm^3). An excess of trimethyl(methoxy)silane was added dropwise to this mixture. Weights and quantities are summarized in Table 1. The reaction mixture was stirred overnight at room temperature. Afterward, volatiles were separated under dynamic vacuum and analyzed with GC-MS. The powder was dried under vacuum at 150 °C overnight. The final powders (labeled as **SiSn-4Me3Si** and **SiSn-7Me3Si** signifying the trimethylsilylation degree) were stored in the dry box (yields in Table 1).

Ethyl Lactate Production: Catalytic Test in the Liquid Phase

A catalytic test was performed under a condenser in a two-necked flask. The flask was filled with 1,3-dihydroxyacetone (0.54 g, 6 mmol in the form of 1,3-dihydroxyacetone dimer), dodecane (68 μl) as internal standard, and ethanol (11.76 g, 0.2552 mmol) acting as a reagent and a solvent. The mixture was heated to 60 °C for 30 min to obtain a homogeneous solution. Meanwhile, the solution was naturally cooled down, and the oil bath was preheated to 90 °C. A tin silicate catalyst (50 mg) was added to the cooled solution, and the flask was returned to the preheated oil bath (90 °C). The tin silicate catalysts were either exposed to the ambient atmosphere (labeled as wet) or dried in an oven overnight at 110 °C (labeled as dry) prior to the catalytic reaction. Aliquots were withdrawn from the reaction mixture via septum and diluted with ethanol. The solutions were analyzed using a gas chromatograph (Scion Instruments 456-GC) equipped with a Restek Stabilwax column (30 m length, 0.53 mm ID, 0.25 μm df) and an flame ionization detector (FID) detector. The components were calibrated with pure chemicals.

Aminolysis of Styrene Oxide by Aniline: Catalytic Test in the Liquid Phase

Styrene oxide (SO) ring opening by aniline was carried out in a batch reactor (i.e., a closed vial). The tin silicate catalysts were either exposed to ambient atmosphere overnight, or dried under dynamic vacuum at 150 °C. First, the catalyst (20−25 mg) was dispersed in toluene (acting both as a solvent and an internal standard). Second, aniline was dropped to the suspension followed by SO addition. The molar ratio of all components n_{Sn}:$n_{toluene}$:$n_{aniline}$:n_{SO} was set to 1:12,000:250:250. The reaction mixture was stirred at 750 rpm at 40 °C in an oil bath. Aliquots were taken after 10, 20, 30, and 60 min, dissolved in benzene-d_6 and analyzed by ^{1}H NMR.

3. RESULTS AND DISCUSSION

3.1. Inorganic Tin Silicates

3.1.1. Synthesis and Characterization of Inorganic Tin Silicates. In the first stage of this study, we elucidated the ideal inorganic tin silicate catalyst for subsequent surface grafting. Amorphous tin silicates were synthesized via the NHSG method using three different types of condensation reactions: alkyl halide elimination, acetamide elimination, and alkyl halide elimination combined with delayed acetamide elimination (Figure 1).

The alkyl halide elimination, ether route is known to provide mesoporous materials[47,48] exhibiting high content of interparticle voids[40,46] leading to large specific surface areas and pore volumes. It has been widely used for metallosilicate preparation,[47,49−52] but its application to synthesize tin silicates (**SiSn-RCl**) has not been reported so far. Herein, the tin silicate synthesis by alkyl halide elimination with nominal n_{Si}:n_{Sn} = 72 (eq 1) shows that tin(IV) tetrachloride is apparently an inappropriate metal precursor as it leads to a high microporosity content (Figure 2A) and practically no tin incorporation in **SiSn-RCl** (no Sn detected with XPS and Sn content below ICP-OES limit of detection after sample mineralization; Table S1). Consequently, no acid sites were observed in **SiSn-RCl** by the infrared spectroscopy combined with pyridine adsorption(IR-py) technique (Figure 2B). Thus, it has been decided to abandon the alkyl halide elimination route.

$$72\ SiCl_4 + SnCl_4 + 146\ ^{i}PrO^{i}Pr \rightarrow 72\ SiO_2{\cdot}SnO_2 + 292\ ^{i}PrCl \quad (1)$$

The acetamide elimination route has already been shown to successfully provide tin silicates in molar ratio n_{Si}:n_{Sn} = 1:1 with a homogeneous Sn-Si mixing.[38] Here, the nominal ratio has been elevated to 72 (**SiSn-Ac**, eq 2) to avoid tin oxide clusters formation and to obtain catalytically active materials. This approach provided well and virtually fully incorporated tin into the silicate matrix (Table 2 and Table S1). Indeed, the tin dispersion is highly homogeneous according to XPS and DR UV–vis (Figure 2C and Figure S1). Briefly, the Sn $3d_{3/2}$ and Sn $3d_{5/2}$ binding energies have been observed at 495.6 and 487.2 eV via XPS (Table S2), respectively, values typical for isolated tin sites in Sn-Beta zeolite.[15,53] Even though structure-directing Pluronic F127 was added, porosity originating in interparticle voids[54] rather than mesoporous character materials[38,40,43,55] with relatively uniform pores[38,43] was obtained (Figure S2). The different hysteresis

Table 1. Synthesis Data for Post-Modified Tin Silicates Prepared by Alkyl Halide Elimination Combined with Delayed Acetamide Elimination

		SiSn-parent		trimethyl(methoxy)silane		
Sample	SiSn-parent temperature pretreatment	m (g)	n_{Sn} (mmol)	m (g)	n (mmol)	yield (g)
SiSn-4Me3Si	500 °C	1.5827	0.354	0.562	5.39	1.6902
SiSn-7Me3Si	room temperature	1.7965	0.401	0.629	6.04	1.5453

https://doi.org/10.1021/acscatal.6c00144
ACS Catal. 2026, 16, 8199−8217

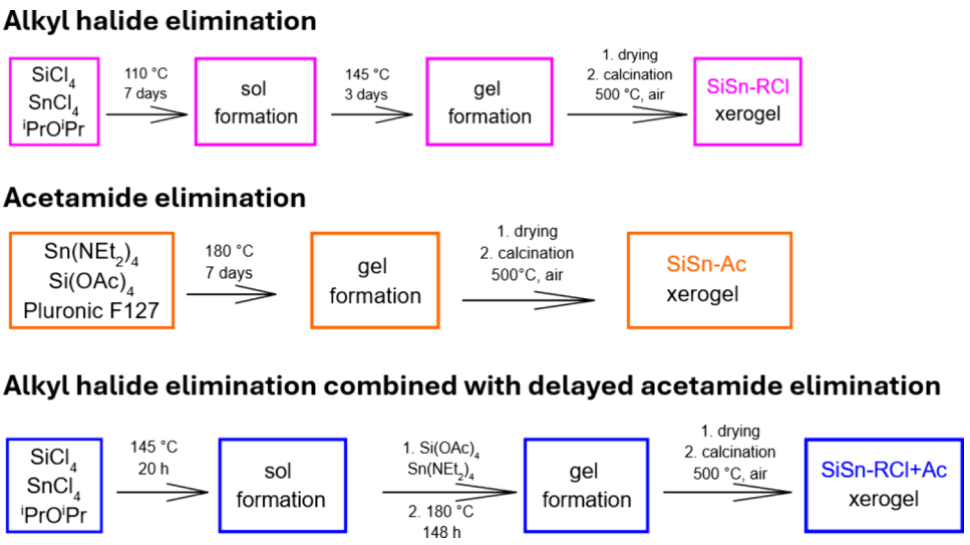

Figure 1. Synthesis scheme for inorganic tin silicates.

(Figure 2A) compared to that typically provided via acetamide elimination can be caused by partial template decomposition at higher temperature. Such a behavior has been already observed for zirconosilicates prepared via templated NHSG synthesis.[56] Nevertheless, specific surface area of 792 $m^2\ g^{-1}$ and total pore volume of 0.95 $cm^3\ g^{-1}$ reached excellent values (Table 2 and Table S3). This in turn led to a Lewis acidic material (confirmed by IR-py (Figure 2B) and IR-CD_3CN; Table 2 and Section 3.1.3 in the Supporting Information, Figures S3−S6, Tables S4−S6) in agreement with other reports on tin silicates.[57−60]

$$72\ Si(OAc)_4 + Sn(NEt_2)_4 \rightarrow 72\ SiO_2{\cdot}SnO_2 + 4\ AcNEt_2 + 142\ AcOAc \quad (2)$$

Finally, the alkyl halide elimination combined with delayed acetamide elimination route is presented here for the first time (**SiSn-RCl+Ac**, eq 3). This two-step synthetic procedure was imagined for three main reasons: (i) To obtain advantageous textural properties without a need to employ a porogen (typical for alkyl halide elimination route),[51] (ii) to achieve a high metal dispersion in silica (usually observed for acetamide elimination),[51] and (iii) to ensure a high tin site accessibility in the surface layer (noticed for NHSG-made aluminosilicates already when applying a delayed metal precursor addition).[61] This approach appeared to be highly successful as per the following observations: (i) full tin incorporation (ICP-OES, Table 2 and Table S1), (ii) homogeneous Sn distribution as determined by XPS (Table S2), STEM-EDS (Figure 2D), and DR UV−vis spectroscopy (Figure S1), (iii) mesoporous character with higher specific surface area, total pore volume, and average pore size diameter without any need for a sacrificial template (Figure S2 and Table 2) compared to other reported tin silicates (Table S3), and (iv) the highest LAS number out of the studied materials according to both IR-py and IR-CD_3CN (Table 2). Acid sites according to IR-py also revealed a different strength of acid sites. The combined elimination route was able to create slightly stronger acid sites in tin silicates but hardly as strong as acid sites in Sn-Beta zeolites.[58] Notably, the efficiency of incorporated Sn in creating acid sites was as high as 92%, (Figure S3 and Table S4), i.e., almost every Sn atom in **SiSn-RCl+Ac** was Lewis acidic, similar to zeolites[62] or Sn-MCM-41.[12] Thanks to the two-steps synthesis, a siliceous network is preformed prior to tin introduction during the first step, alkyl halide elimination with limited tin amount, while most of the tin is then homogeneously distributed in the surface layer via acetamide elimination in the second step (Table S5).

$$9\ Si(OAc)_4 + 63\ SiCl_4 + 0.1\ SnCl_4 + 0.9\ Sn(NEt_2)_4 + 110\ {}^{i}PrO{}^{i}Pr \rightarrow 72\ SiO_2{\cdot}SnO_2 + 220\ {}^{i}Pr^{Cl} + 3.6\ AcNEt2 + 32.4\ AcCl \quad (3)$$

As already mentioned, the acidity of tin silicates was investigated by two different probes—trideuterated acetonitrile and pyridine. On one hand, acetonitrile-d_3 is a suitable probe to distinguish among open, closed, speculative $Sn(OH)_2$, and SiOH sites via observation of absorption bands at wavenumbers 2316, 2308, 2275, 2287, and eventually 2265 cm^{-1} (CD_3CN in gas phase), respectively.[57] Alternatively, the band at 2287 cm^{-1} can be associated with the presence of extraframework polymeric species (i.e., tin oxide clusters).[63] These bands are usually overlapping peaks (Figure S4), which are usually more distinct for zeolites in comparison to amorphous materials studied herein.[23,57] Noteworthy, the exact distinction between open and closed Sn sites remains controversial.[57,63] In fact, the most recent study combined IR-CD_3CN and DFT calculations and the authors argued that the narrow spectral window (~10 cm^{-1}) and coexistence of structurally different positions in zeolites hinder straightforward assignments of open and closed sites. The system complexity thus requires more nuanced characterization methods.[64]

These uncertainties are further intricate by the sensitivity of open sites to the pretreatment conditions as vacuum and temperature above 400 °C are likely to destabilize Sn−OH species[65] and thus most CD_3CN absorption bands may arise from closed sites in a distinct Sn environment after vacuum/temperature treatment. The transformation of open to closed sites at 400 °C was not observed in this study (Table S6, Figures S5 and S6A). However, tin silicates exhibited comparable total acid site amount when evaluated by both acetonitrile and pyridine adsorption (Figure S6B) indicating consistent

https://doi.org/10.1021/acscatal.6c00144
ACS Catal. 2026, 16, 8199−8217

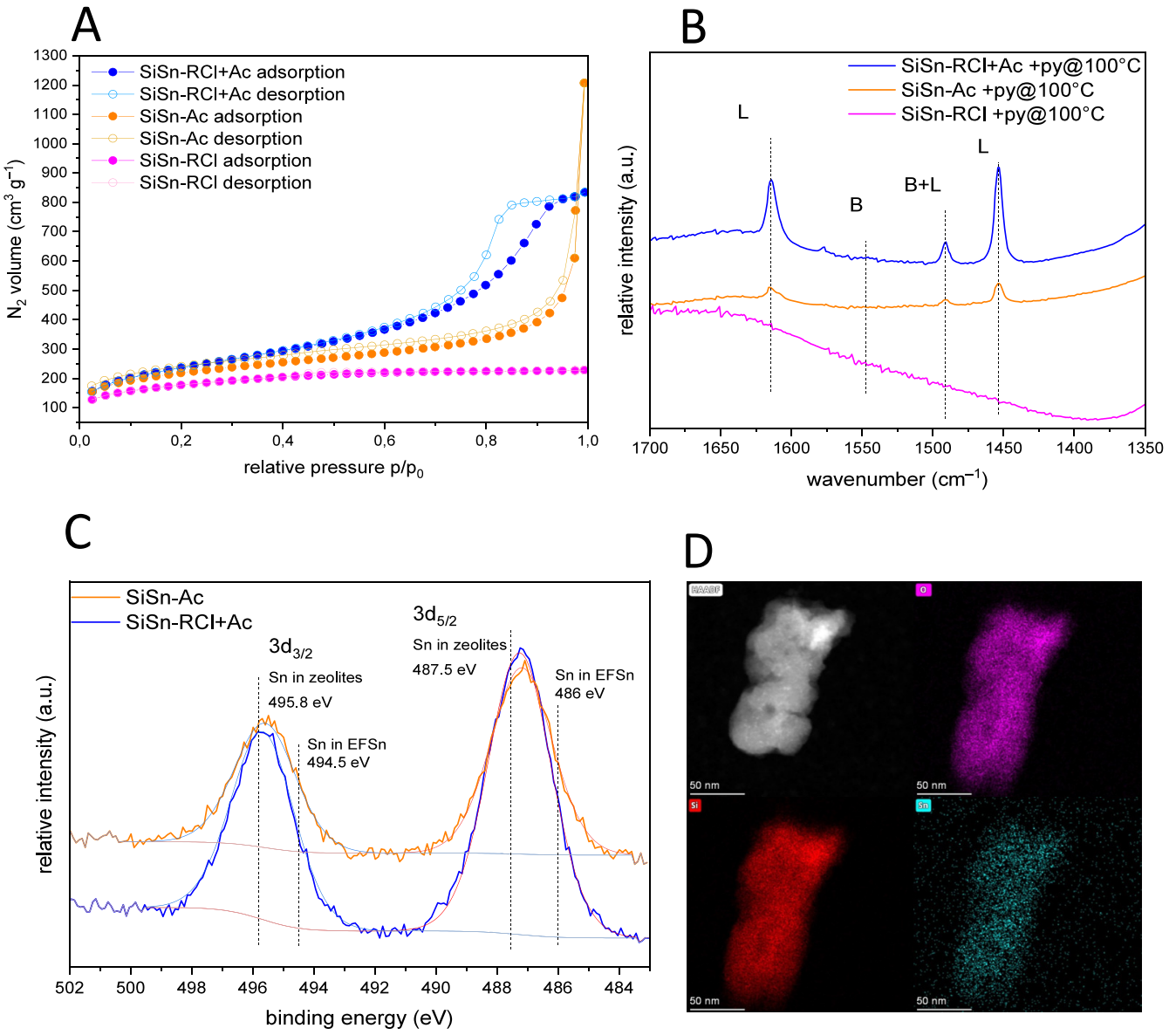

Figure 2. (A) N_2 adsorption desorption isotherms, (B) IR spectra upon IR-py analysis, pyridine desorbed at 100 °C indicating pyridine chemisorption on Lewis acid sites (1454 cm^{-1}, 1491 cm^{-1}, and 1614 cm^{-1}), (C) high-resolution Sn 3d XPS of **SiSn-Ac** and **SiSn-RCl+Ac** displaying a doublet with binding energies of 495.7 (Sn $3d_{3/2}$) and 487.3 eV (Sn $3d_{5/2}$) and 495.6 (Sn $3d_{3/2}$) and 487.2 eV (Sn $3d_{5/2}$) for **SiSn-RCl+Ac** and **SiSn-Ac**, respectively, indicating the presence of "zeolite-like" Sn sites (495.8 and 487.5 eV)[15] rather than extraframework tin (EFSn) species (486.0 and 494.5 eV),[20] and (D) STEM-EDS of SiSn-RCl+Ac indicating well-dispersed Sn sites in the silicate matrix.

Table 2. Elemental Composition, Textural Properties, and Acid Site Concentration of Inorganic Tin Silicates

Sample	SiSn-RCl	SiSn-Ac	SiSn-RCl+Ac
$c_{Sn,ICP\text{-}OES}$ (mmol g^{-1})	<0.0067	0.133	0.291
SA_{BET} (m^2 g^{-1})	639	792	852
V_{total} (cm^3 g^{-1})	0.35	0.95	1.3
[a]LAS_{100} (mmol g^{-1})	0	0.078	0.269
[b]$LAS_{open+closed}$ (mmol g^{-1})		0.035	0.14

[a]LAS concentration after pyridine desorption at 100 °C determined by IR-py. [b]LAS concentration after CD_3CN desorption at room temperature determined by IR-CD_3CN.

trends regardless of the used probe.[57] Since the overlapping nature of acetonitrile bands is pronounced in the case of amorphous tin silicates (Figure S4), combined with general ambiguity of peak assignment, IR-CD_3CN is less reliable, and its interpretation must be taken with caution. Instead, a more complex approach, like computational studies, would be demanded to specifically elucidate the LAS character.

Thus, we have decided to rely on Lewis acidity determined by pyridine. The pyridine desorption at 100 °C (Figure S6C) was chosen to evaluate turnover frequency, $TOF_{LAS,100}$, as (i) no physisorbed pyridine was present, (ii) tin utilization was the highest ($c_{Sn,ICP\text{-}OES}$ vs. LAS_{100}), and (iii) both catalytic reactions were performed at low temperatures.

https://doi.org/10.1021/acscatal.6c00144
ACS Catal. 2026, 16, 8199−8217

3.1.2. Catalytic Activity of Inorganic Tin Silicates. Catalytic performance was tested in two different reactions where hydrophobicity plays the role[29,66] (see Sections 3.2.3 and 3.2.4). The first one, DHA transformation to EL (Figure 3), is known to be catalyzed by LAS, e.g., tin silicates with homogeneously distributed tin atoms. Side reactions are usually triggered by strong Brønsted acid sites (Figure S7). Among the synthesized tin silicates, those prepared by alkyl halide elimination combined with delayed acetamide elimination provided the highest EL yield (**SiSn-RCl+Ac**; 16% after 6 h) compared to tin silicate prepared by acetamide elimination (**SiSn-Ac**; 6% after 6 h; Table 3 and Figure S8). The EL yield over **SiSn-RCl+Ac** was also comparable with that over mesoporous amorphous tin silicates prepared elsewhere (Tables S7 and S8).[35] The explanation can be found in Lewis acidity as the LAS numbers were higher in the case of **SiSn-RCl+Ac** compared to **SiSn-Ac** (Table 2 and Table S6). Interestingly, an apparent turnover frequency ($TOF_{EL,LAS,100}$) showed a similar efficiency of catalytic sites in **SiSn-Ac** and **SiSn-RCl+Ac** (Table 3 and Figure S8), further confirming that catalysis was triggered by Lewis acidity as reported elsewhere.[12] The catalytic activity comparison of catalysts prepared in the literature is summarized in Table S8.

The second catalytic reaction, epoxide ring opening by aniline (Figure 4), was performed over **SiSn-Ac** and **SiSn-RCl+Ac**. Both **SiSn-Ac** and **SiSn-RCl+Ac** maintained selectivity between 95 and 98% to the Markovnikov product. However, **SiSn-RCl+Ac** was more active compared to **SiSn-Ac** (Table 3 and Figure S9A). This can be again explained by higher LAS numbers in **SiSn-RCl+Ac** compared to **SiSn-Ac**. Similarly to EL production, the apparent turnover frequency ($TOF_{SO,LAS,100}$) was comparable for both samples (Table 3 and Figure S9B).

The results discussed above show that both **SiSn-Ac** and **SiSn-RCl+Ac** are active catalysts in EL synthesis and epoxide ring aminolysis. Importantly, the catalytic activity of their acid sites is similar. The dramatic difference between the samples is directly related to the LAS numbers. Thanks to a high Sn surface concentration, high Sn dispersion in a silicate matrix, and large open porosity (V_{total} = 1.3 $cm^3\ g^{-1}$), the **SiSn-RCl+Ac** sample achieved high acid site numbers and, accordingly, high activities in both tested reactions. Therefore, **SiSn-RCl+Ac** has been chosen for further studies on surface hydrophobization.

3.2. Surface Modification of Tin Silicate

Surface hydrophilicity/hydrophobicity often has a dramatic impact on catalytic activity.[27,66,68] Both studied catalytic reactions could be sensitive to hydrophilicity/hydrophobicity of the catalyst surface: (i) water is formed when DHA is dehydrated during EL production[29,35,69] and (ii) nonpolar bulky organic molecules[70,71] participate in SO aminolysis. Therefore, the surface of tin silicate prepared by alkyl halide elimination coupled with delayed acetamide elimination was functionalized with hydrophobic trimethylsilyl groups.

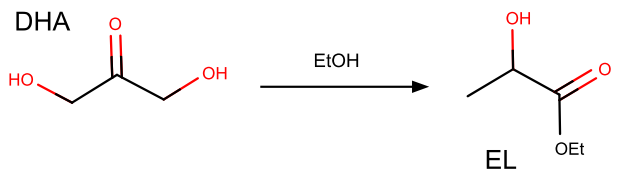

Figure 3. Dihydroxyacetone transformation into ethyl lactate, detailed reaction scheme is provided in the Supporting Information.

Table 3. Catalytic Performance of Inorganic Tin Silicates

	SiSn-RCl[e]	SiSn-Ac	SiSn-RCl+Ac
DHA transformation to EL			
[a]Y_{EL} (%)	0	6	16
[b]$TOF_{EL,LAS,100}$ (h^{-1})		17	13
epoxide ring opening by aniline			
[c]X_{SO} (%)		23.5	32.5
[d]$TOF_{SO,LAS,100}$ (h^{-1})		225	175

[a]Ethyl lactate yield after 6 h. [b]Turnover frequency based on EL produced per acid site number determined by IR-py (py desorption temperature 100 °C) (derived upon 6 hours of catalysis). [c]Styrene oxide conversion after 60 min. [d]Turnover frequency based on styrene oxide converted per acid site number determined by IR-py (derived upon 10 min of catalysis). [e]Inactive sample although specific surface area reached 639 $m^2\ g^{-1}$ but LAS were missing due to the unsuccessful tin incorporation. The Si−OH groups on the surface themselves were not able to convert DHA as weakly acidic silanol groups in the near Sn environment play a decisive role in the catalytic DHA transformation. Si−OH moieties and LAS based on well-inserted tin in silicate matrix can synergistically complement each other.[12]

Trimethyl(methoxy)silane (Me_3SiOMe) served as a source of hydrophobic groups (Figure 5) similar to a previous study on aluminosilicates.[66] Prior to chemical modification, pristine tin silicate prepared by alkyl halide elimination combined with delayed acetamide elimination (new batch with Si:Sn ratio equal to 89 − **SiSn-parent**, the synthesis was performed in the same way as **SiSn-RCl+Ac** in part 3.1, Table 2) was pretreated under dynamic vacuum either at room temperature or at 500 °C. **SiSn-parent** pretreatment at two different temperatures provided two modified samples with a varying number of trimethylsilyl groups after reaction with trimethyl(methoxy)-silane: **SiSn-7Me3Si** and **SiSn-4Me3Si** (pretreatment at room temperature and 500 °C, respectively; Figure 5). Numbers 7 and 4 in the sample labels indicate the relative amount of trimethylsilyl groups with respect to all silicate components determined by ^{29}Si MAS NMR (vide infra).

During the trimethylsilyl groups grafting, methanol elimination (eq 4) was confirmed by GC-MS. No methanol dehydration product was revealed (due to ambient temperature during the reaction), and thus in situ water production was excluded. However, 1,1,1,3,3,3-hexamethyldisiloxane was detected as a consequence of a reaction between trimethyl(methoxy)silane and water remaining in the pores and subsequent condensation (eq 5 and 6, respectively).[66] Finally, the excessive trimethyl(methoxy)silane added into a pretreated tin silicate material was observed in volatiles after reaction by GC-MS.

$$\equiv SiOH + Me_3Si - OMe \rightarrow \equiv SiOSiMe_3 + MeOH \quad (4)$$

$$MeOSiMe_3 + H_2O \rightarrow MeOH + Me_3SiOH \quad (5)$$

$$Me_3SiOH + Me_3SiOH \rightarrow Me_3SiOSiMe_3 + H_2O \quad (6)$$

Attenuated-total reflectance infrared spectroscopy (ATR-IR) confirmed that silanol SiOH groups were replaced by Me_3Si groups. The absorption band at 960 cm^{-1} representing the deformation vibration of Si−O−H is present in **SiSn-parent** but diminished in the case of modified samples (Figure 6A). Instead, new symmetric and asymmetric rocking absorption

https://doi.org/10.1021/acscatal.6c00144
ACS Catal. 2026, 16, 8199−8217

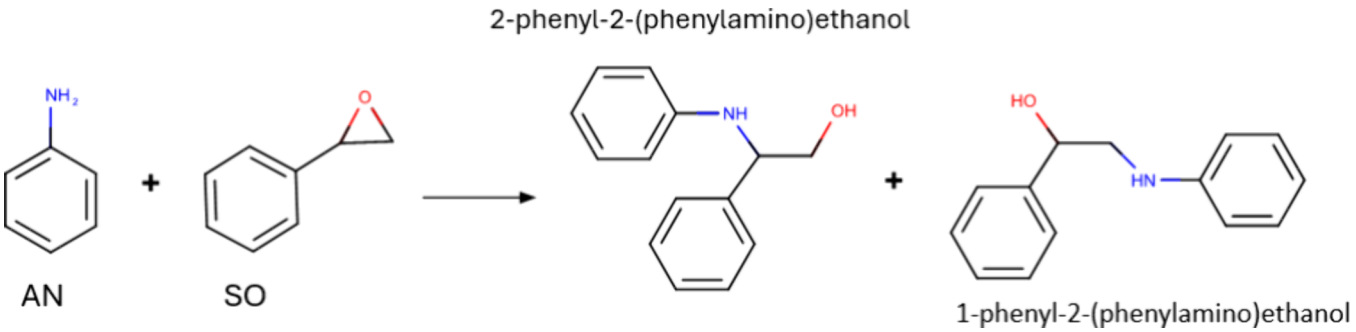

Figure 4. Scheme of styrene oxide (SO) aminolysis catalyzed by acid metallosilicate catalysts (Sn,[38] Ti,[67] Al,[43] and Zr[55]) producing two major products. Either aniline (AN) attacks the more substituted carbon of SO ring and 2-phenyl-2-(phenylamino)ethanol is produced, or it attacks the other one and forms 1-phenyl-2-(phenylamino)ethanol. The former product is usually yielded with higher selectivity.

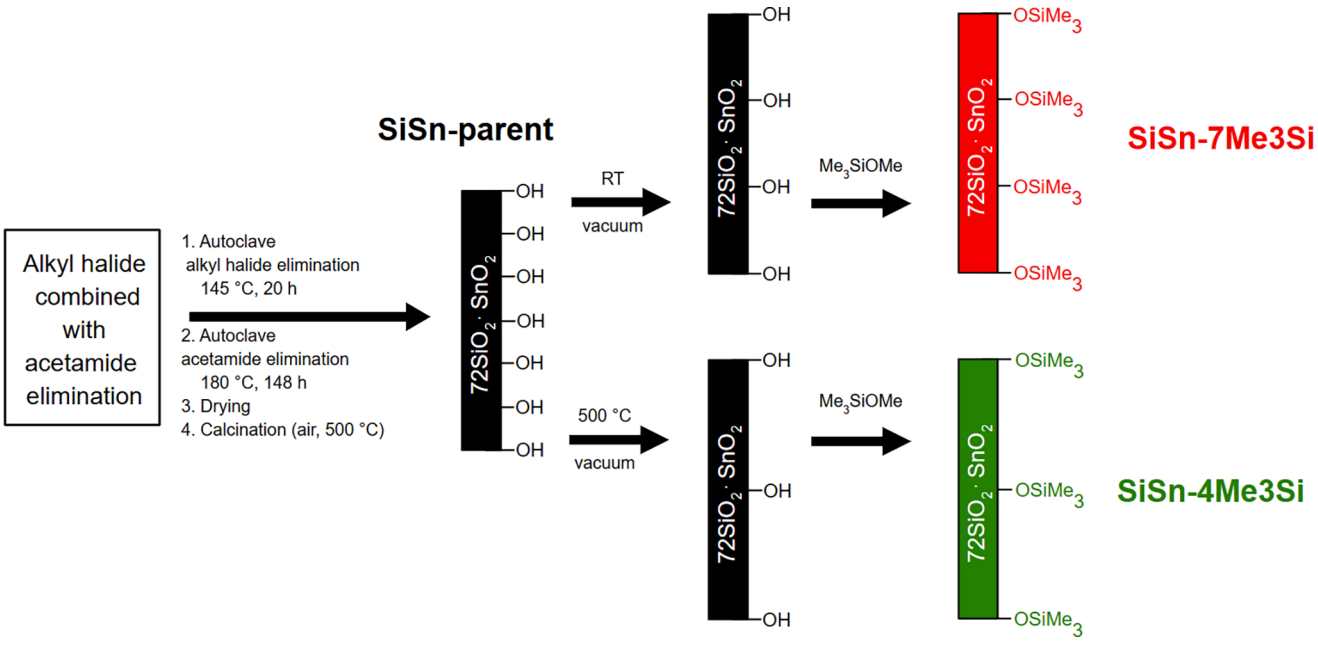

Figure 5. Modification of tin silicate samples prepared by NHSG condensation, particularly alkyl halide elimination combined with delayed acetamide elimination.

bands of $SiCH_3$ appeared (759 and 847 cm^{-1}) supporting a successful OH modification.

The Fourier-transform infrared spectra (FTIR) of degassed samples at 250 and 400 °C were recorded for closer evaluation of O−H and C−H stretching vibration modes. The lattice vibration overtones and combination bands between 2100 and 1750 cm^{-1} did not change significantly (Figure S10) upon trimethylsilylation, so that a direct comparison is possible. Observation of O−H and C−H vibrations of degassed samples (Figure 6B) supports successful OH groups replacement by $SiMe_3$ groups. The IR difference spectra of hybrid tin silicates relative to **SiSn-parent** (Figure S11) indicate that the modifying agent reacted with several types of SiOH groups. First, the broad band attributed to hydrogen bonded SiOH[72] (with maximum ~3590−3570 cm^{-1}) decreased upon modification[73] to a similar extent for both **SiSn-4Me3Si** and **SiSn-7Me3Si** when dried at both 250 and 400 °C. Second, the absorption band at 3735 cm^{-1} was also affected with a more pronounced decrease observed for the heavily trimethylsilylated sample.[79] This band can be assigned to several species according to the literature: geminal,[74] terminal,[75] or internal[76−78] SiOH groups. The assignment to geminal moieties is preferred as it is corroborated by results obtained by ^{29}Si MAS NMR where the Q^2 signal diminished upon reaction with trimethyl(methoxy)silane (discussion below).

In contrast, isolated[72] (terminal) SiOH groups at 3745 cm^{-1} seem to be less reactive toward a silylating agent. Their intensity remained unchanged for **SiSn-7Me3Si** dried at 400 °C and slightly increased for **SiSn-4Me3Si** when dried at 250 and 400 °C. The latter phenomenon may result from disruption of hydrogen bonded silanols by attachment of trimethylsilyl groups and thus from the formation of new isolated silanols. Overall, silanol content appears to decrease in the order **SiSn-parent>SiSn-4Me3Si>SiSn-7Me3Si**. In the opposite direction the intensity of symmetric and asymmetric C−H vibration (3000−2800 cm^{-1}) increased as trimethylsilyl groups replaced OH groups.

The effects of trimethylsilylation were also studied by solid state NMR. The ^{29}Si MAS NMR spectrum of the parent tin

https://doi.org/10.1021/acscatal.6c00144
ACS Catal. 2026, 16, 8199−8217

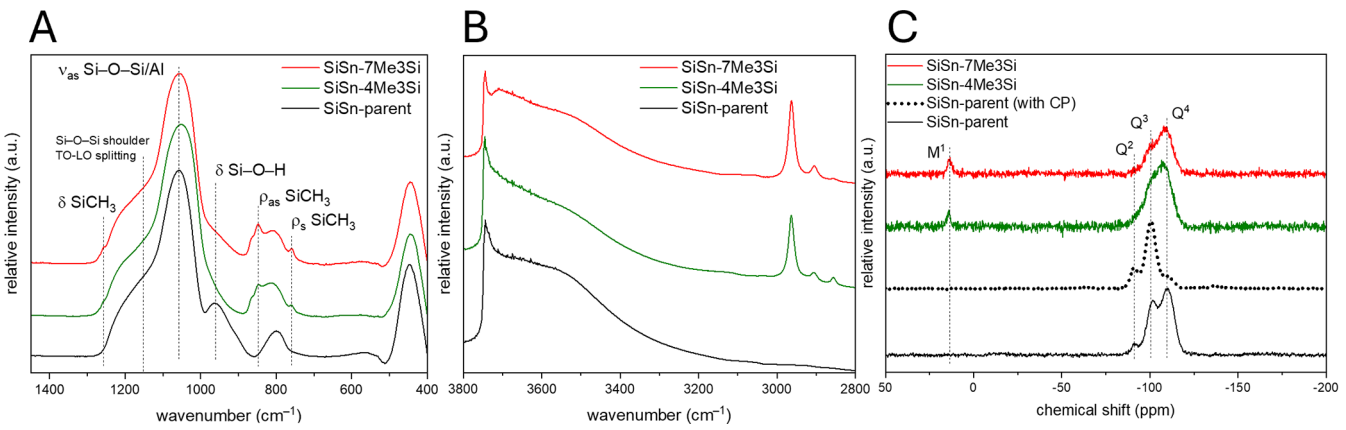

Figure 6. ATR-IR spectra signalizing the presence of asymmetric vibration of Si−O−Si/Al with a typical shoulder for silica-based materials (1150 cm^{-1}) related to TO-LO splitting[84] (A); FTIR spectra of OH and CH region of degassed samples at 250 °C under dynamic vacuum (B); ^{29}Si (solid lines) and ^{29}Si CP (dotted line) MAS NMR spectra (C) of pristine tin silicate samples and modified by trimethyl(methoxy)silane.

silicate (Figure 6C) is dominated by a broad resonance at approximately −110 ppm corresponding to Q^4 sites; however, due to the low tin content, it was not possible to distinguish between $Si(OSi)_4$ and $Si(OSi)_3(OSn)$ environments. Less intense signals representing Q^3 ($Si(OSi)_3OH$) and Q^2 ($Si(OSi)_2(OH)_2$ sites were observed at approximately −100 and −90 ppm, respectively.[80,81] To clarify these assignments, ^{29}Si cross polarization (CP) MAS NMR was employed, where Q^3 and Q^2 signals become dominant and intensity is significantly enhanced. This enhancement occurs because the signal intensity for silicon atoms bonded to hydroxyl groups is boosted via magnetization transfer from nearby protons to the silicon nuclei. Consequently, sites associated with silanol groups exhibit much stronger relative intensities in the CP MAS spectrum compared to the direct excitation in standard ^{29}Si MAS NMR.

For the tin silicate materials modified with trimethylsilyl groups, a significant decrease in the intensity of the Q^2 signals was observed in the ^{29}Si MAS NMR spectra. Furthermore, a new resonance appeared at 14 ppm, originating from the surface modification by trimethylsilyl groups.[82] The deconvolution of the ^{29}Si MAS NMR spectra to Q^2, Q^3, and Q^4 signals revealed that the relative amounts of individual Q^n species changed upon grafting (Table S9). While Q^2 tetrahedra of **SiSn-parent** represented 7% of the total Q sites, trimethylsilylation converted them into Q^3 (**SiSn-4Me3Si**) and Q^4 (**SiSn-7Me3Si**) tetrahedra.

The amount of trimethylsilyl groups attached to the surface varied depending on the sample, specifically on the temperature-vacuum pretreatment of pristine tin silicate prior to modification. While **SiSn-4Me3Si** stemming from **SiSn-parent** dehydrated at 500 °C provided 4% of M^1 with respect to all tetrahedra, **SiSn-7Me3Si** derived from **SiSn-parent** dehydrated at room temperature contained 7% M^1 units (Table 4). Thus, temperature-vacuum pretreatment of **SiSn-parent** enables the control of the concentration of Me_3Si groups on the tin silicate surface, similarly to our earlier report on aluminosilicates hydrophobization.[66] High resolution XPS analysis of the Si 2p region (Figure S12A) corroborated ^{29}Si MAS NMR spectra and showed a higher amount of C_3SiO species in **SiSn-7Me3Si** compared to **SiSn-4Me3Si** (Table S10).[83] The differences in the amount of attached Me_3Si groups on the surface were also confirmed by thermal gravimetry combined with differential scanning calorimetry (TG/DSC, Figure S12B).

Besides the expected signal for trimethylsilyl groups at 2 ppm, the ^{13}C CP MAS NMR spectrum (Figure S12C) showed a weak signal of methoxy groups (53 ppm).[85] These may form through coordination or hydrogen bonding between methanol and acid sites, or via exchange reaction (eq 7) as reported elsewhere.[66,86]

$$\equiv SiO-Si\equiv + Me_3Si-OMe \rightarrow \equiv SiO-SiMe_3 + \equiv Si-OMe \quad (7)$$

3.2.1. Effect of Surface Modification on Textural Properties and Hydrophobicity of the Surface. The adsorption and desorption isotherms of **SiSn-4Me3Si** and **SiSn-7Me3Si** closely resemble the isotherm of **SiSn-parent** but show a uniform shift throughout the whole range of relative pressures to lower adsorbed volumes (Figure 7A). Apparently, micropores were occupied by trimethylsilyl groups, as corroborated by t-plot analysis. Micropore contribution dropped from 4.8% in **SiSn-parent** down to 2.9 and 0.7% for **SiSn-4Me3Si** and **SiSn-7Me3Si**, respectively (Table 5). Such a decrease of microporosity upon trimethylsilylation was also observed in

Table 4. Influence of Dehydration Temperature of Matrix on the Percentual Integrated Peak Area of Trimethylsilyl Groups on the Surface Determined According to ^{29}Si MAS NMR Spectra and Elemental Composition of synthesized tin silicates determined by XPS and ICP-OES

sample	dehydration temperature of SiSn-parent	relative integrated area of Me_3Si (%)	$n_{Si}:n_{Sn}$ (ICP-OES/XPS)	$c_{Sn,ICP\text{-}OES}$ (mmol g^{-1})
SiSn-parent			89/138	0.139
SiSn-4Me3Si	500 °C	4	108/149	0.132
SiSn-7Me3Si	room temperature	7	88/131	0.131

https://doi.org/10.1021/acscatal.6c00144
ACS Catal. 2026, 16, 8199−8217

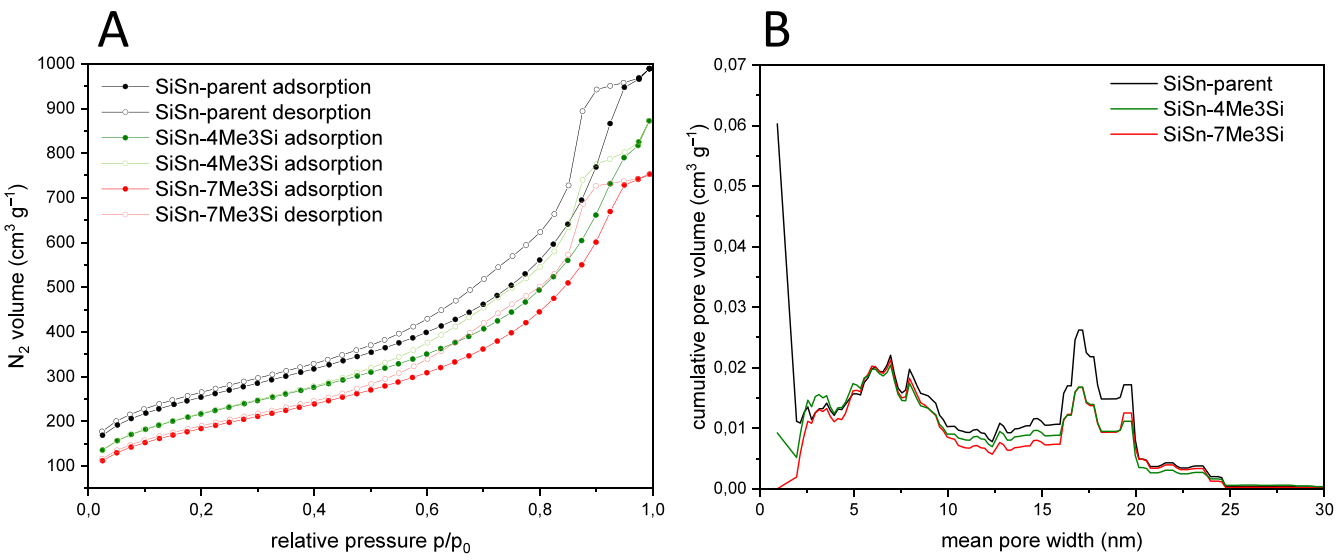

Figure 7. Nitrogen isotherms (A), pore size distribution determined by calculation via the NLDFT equilibrium model considering silica adsorbent and cylindrical pores (B) of pristine tin silicate and trimethylsilylated samples.

Al-zeolites.[73] The pore size distribution also shows a notable volume reduction in the micropore range, i.e., <2 nm (Figure 7B). Accordingly, the total pore volume and specific surface area of tin silicates after Me_3Si groups grafting dropped with increasing Me_3Si content (Table 5). A similar trend was observed in NHSG-prepared aluminosilicates modified with trimethyl(methoxy)silane under the same conditions.[66]

The hydrophobic properties were investigated by water adsorption porosimetry (Figure 8A). As a result, the percentual representation of adsorbed water after modification has not changed. The hydrophilicity index at the relative pressure $p/p_0 = 0.3$[87,88] ($X_{0.3}$) remained similar–24, 28, and 23% for **SiSn-parent**, **SiSn-4Me3Si**, and **SiSn-7Me3Si**, respectively. These results are in striking contrast to recently reported data on trimethylsilylated aluminosilicates prepared in a similar way, where modified materials adsorbed significantly less water than the parent inorganic aluminosilicate sample.[66]

Water contact angle (WCA) was measured on **SiSn-parent**, **SiSn-4Me3Si**, and **SiSn-7Me3Si** to further investigate the influence of trimethylsilyl groups on the surface polarity (Figure 8B–D). A water drop carefully placed onto the **SiSn-parent** pellet was difficult to catch as it quickly disappeared. Thus, water contact angle was less than 10° indicating a highly hydrophilic surface. On the other hand, the contact angles on the interfaces of water and surface of **SiSn-4Me3Si** and **SiSn-7Me3Si** were around 47 and 36°, respectively. Higher WCAs indicate a more hydrophobic surface compared to **SiSn-parent**. These materials are more hydrophobic in comparison to methylsilyl-functionalized aluminosilicates prepared in one-pot.[61] The differences in results of water adsorption porosimetry and WCA can be caused by significant differences between the analytical methods and different pretreatment before analysis.

3.2.2. Effect of Surface Modification on Tin Nature and Acidity. The **SiSn-parent** sample exhibited highly homogeneous tin dispersion (see Section 3.1). According to UV–vis spectroscopy (Figure S13A), the sample contained distorted tetrahedral or pentacoordinated Sn atoms, as well as a low amount of small extraframework species, as derived from the presence of absorption bands between 200 and 245 nm in the spectra.[89] Tin speciation was further examined using XPS analysis. The Sn 3d high resolution XPS spectra (Figure S13B) revealed a doublet with binding energies of Sn $3d_{3/2}$ and Sn $3d_{5/2}$ at 495.7 eV and 487.3 eV, respectively (Table S10). These values are very close to binding energies observed in Sn-Beta zeolite confirming an outstanding tin dispersion in the amorphous silica matrix.[15,53] After surface modification, the Sn 3d binding energies remained comparable to the **SiSn-parent** sample (Figure S13B and Table S10) suggesting negligible change in tin speciation upon reaction with trimethyl(methoxy)silane.

Tin silicate acidity was investigated by IR-py analysis (Figure 9). Interaction of OH groups and tin sites with pyridine in the **SiSn-parent** and modified **SiSn-4Me3Si** and **SiSn-7Me3Si** revealed acid site nature, strength, and concentration. First, at the desorption temperature of 50 °C, absorption bands at 1445 cm^{-1} (hydrogen bonded pyridine), 1454 cm^{-1} (LAS), 1491 cm^{-1} (Brønsted acid sites and LAS), 1577 cm^{-1} (weak Lewis bound pyridine[90,91] or physisorbed pyridine[92]), 1596 cm^{-1} (hydrogen bonded pyridine), and 1614 cm^{-1} (Brønsted acid sites and LAS) (Figure S14, with detail in

Table 5. Textural Properties of Tin Silicate Matrix SiSn-parent and Its Surface-Modified Hybrids SiSn-4Me3Si and SiSn-7Me3Si

sample	SA_{BET} (m^2 g^{-1})	SA_{micro} (m^2 g^{-1})	SA_{ext} (m^2 g^{-1})	[a]V_{total} (cm^3 g^{-1})	[b]D (nm)	V_{micro}/V_{total}
SiSn-parent	914	178	737	1.49	6.5	4.8
SiSn-4Me3Si	788	99	686	1.26	6.4	2.9
SiSn-7Me3Si	673	35	635	1.15	6.8	0.7

[a]Total pore volume at $p/p_0 = 0.97$. [b]Average pore width $D = 4 \times V_{total}/SA_{BET}$.

https://doi.org/10.1021/acscatal.6c00144
ACS Catal. 2026, 16, 8199–8217

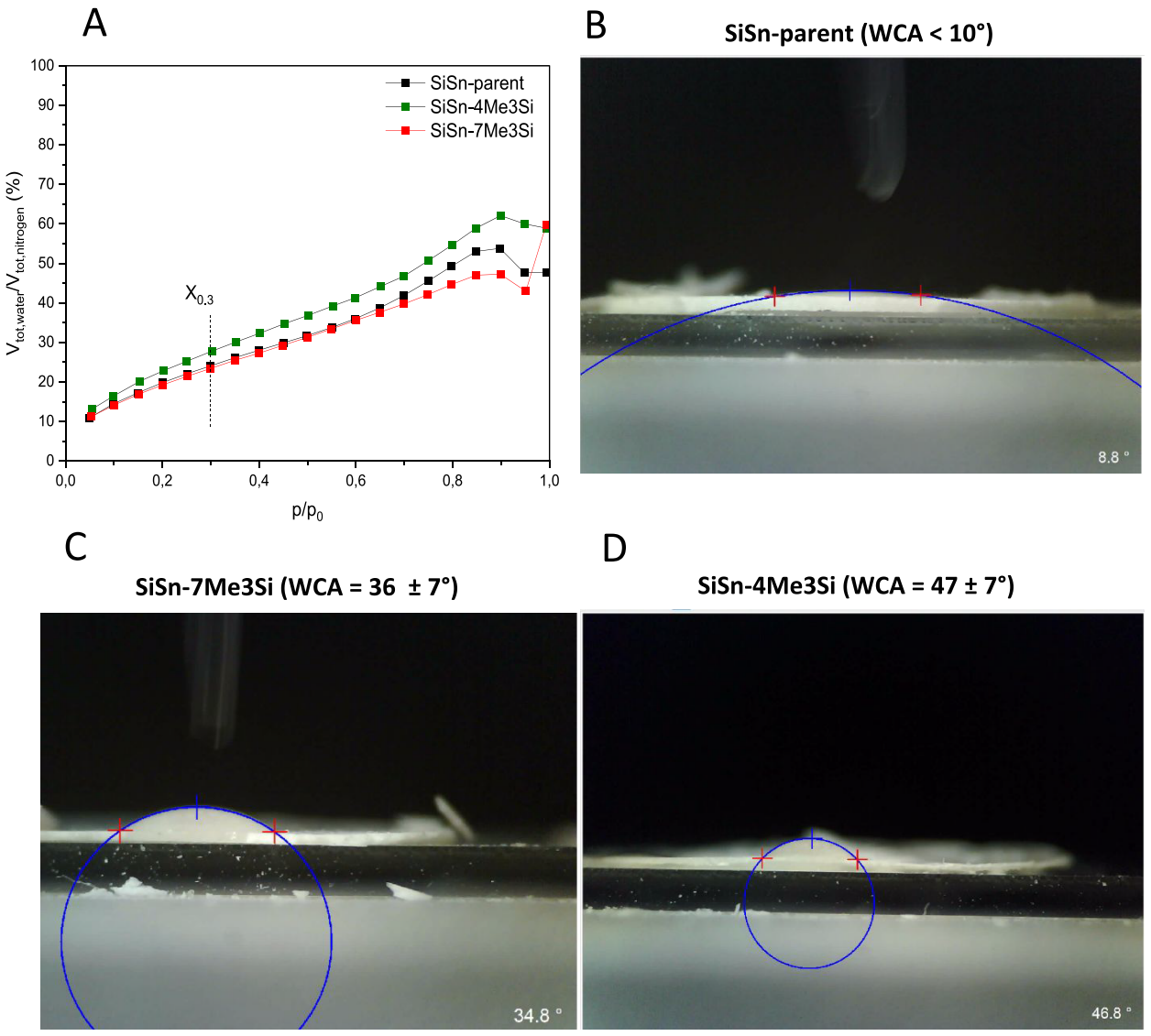

Figure 8. Water adsorption porosimetry (A, results expressed as percentual water vapor pore filling); water contact angle measurements for SiSn-parent (B), SiSn-4Me3Si (C), and SiSn-7Me3Si (D). WCA average numbers based on five measurements and the best captured image for each sample.

Figure S15) were detected. Only Lewis acid bound pyridine was observed after desorption at 100 °C (Figure 9 and Figure S14 right) and higher temperatures (see discussion on number and strength of acid sites below).

Concomitantly with pyridine adsorption, absorption bands between 3800 and 3000 cm^{-1} changed indicating the pyridine interaction with OH groups (Figure S14). While the changes in hydrogen bonded SiOH groups (3200−3600 cm^{-1}) remained similar for both pristine and modified tin silicates, the changes at higher wavenumbers (3800−3700 cm^{-1}) differed among the samples. Differential spectra (Figure S14 left) showed a significant increase in the absorption band related to hydrogen bonded SiOH groups after pyridine adsorption (with maxima at 3680 and 3540 cm^{-1} for **SiSn-parent**, 3520 cm^{-1} for **SiSn-4Me3Si**, and 3690 and 3510 cm^{-1} for **SiSn-7Me3Si**). This interaction was expected as hydrogen bonded pyridine was observed in the spectra after evacuation at 50 °C. Similar behavior has already been reported for Al-zeolites.[93] The bands in the region 3200−3600 cm^{-1} decreased with desorption temperature. Notably, the differences in hydrogen bonded SiOH (region at 3200−3600 cm^{-1}) were still present even when the absorption band related to hydrogen bonded pyridine (1455 and 1596 cm^{-1}) diminished at 100 and 150 °C (Figure S14 right). The absorption band (3200−3600 cm^{-1}) decreased in intensity until the desorption temperature of 250 °C when pyridine was desorbed from all sites (including Lewis acid sites; compare the region of 1700−1400 cm^{-1} with 3600−3200 cm^{-1}, Figure S14, left vs. right). Thus, we assume that persistent hydrogen bonded OH groups during pyridine adsorption and desorption must be related to hydroxyl groups close to the tin sites. Weakly acidic silanol in the proximity of the tin was also identified in Sn-MCM-41.[12] Importantly, the differential spectra in the pyridine region (Figure S14, right) did not clearly prove the presence of Brønsted acid sites at 1545 cm^{-1}. Thus, we speculate that the broad band 3200−3600 cm^{-1} is related to the presence of O_3SnOH and/or $O_2Sn(OH)_2$ species (see discussion below). However, a clear distinction between SiOH groups in close proximity to Sn sites, O_3SnOH and/or

https://doi.org/10.1021/acscatal.6c00144
ACS Catal. 2026, 16, 8199−8217

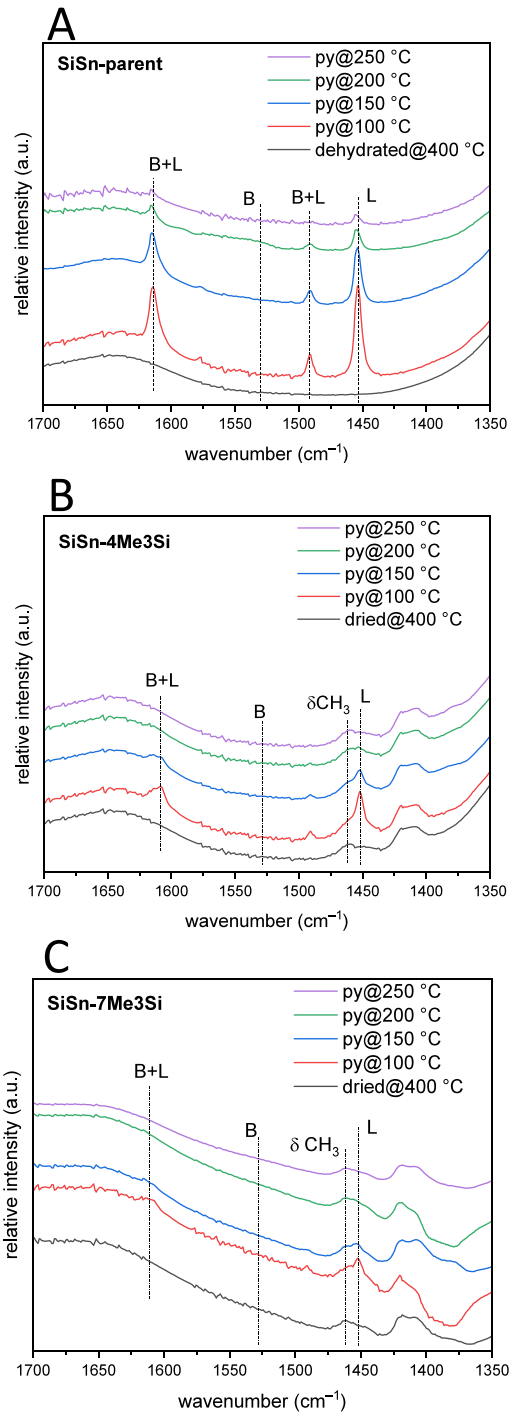

Figure 9. IR spectra of SiSn-parent (A), SiSn-4Me3Si (B), SiSn-7Me3Si (C) after pyridine adsorption desorbed at different temperatures (100, 150, 200, and 250 °C).

$O_2Sn(OH)_2$ species is impossible: (i) The OH region in IR spectra of amorphous tin silicates (both pristine and modified) is composed of broad and overlapping bands without any sharp and clear maxima and (ii) no absorption band of valence OH vibration has been unambiguously assigned to SnOH species in Sn-zeolites containing open acid sites to the best of our knowledge.[7,15,94]

The 3800−3600 cm^{-1} region, corresponding to various SiOH species, also interacted with pyridine as indicated by the negative band in differential spectra (Figures S14 and S15). Isolated silanols (3745 cm^{-1}) of **SiSn-parent** interacted with pyridine (i.e., exhibited a negative intensity in differential spectra) and were liberated at higher desorption temperatures. In the case of surface-modified samples, pyridine adsorption behaved slightly differently (Figure S14B,C) as silylation caused hydrophobic changes in the pore environment. The absorption band of isolated silanols increased in intensity probably due to pyridine adsorption on hydrogen bonded silanols. This could induce the disruption of hydrogen bonding between the silanol groups and the formation of isolated silanol groups (as only a limited number of OH groups were present in modified samples). OH groups exhibiting the absorption band at 3735 cm^{-1} (Figure S15) were occupied by pyridine adsorption in modified samples as it exhibited a negative intensity in differential spectra (compare with **SiSn-parent** where isolated SiOH groups were affected). This band (3735 cm^{-1}) can be assigned to geminal SiOH groups.[74] Interestingly, geminal groups have already been reported to exhibit a stronger hydrogen bonding than isolated silanols toward H_2O as an adsorption probe.[74]

In a nutshell, pyridine adsorption induced significant redistribution/conversion of silanol species in the OH stretching region. In the parent tin silicate, pyridine primarily interacted with accessible silanols, converting isolated SiOH groups into hydrogen bonded hydroxyl moieties. Silanol fraction at 3735 cm^{-1} remained unaffected, indicating limited accessibility. After surface silylation, the silanol network (especially hydrogen bonded SiOH groups) was partially disrupted and spatially isolated, leading to the formation of additional isolated SiOH groups upon probe adsorption. Importantly, the OH region exhibited changes even when only Lewis acid sites were occupied by pyridine indicating the presence of some type of bonding between Lewis acid sites and OH groups.

Finally, all samples exhibited only pyridine bound to Lewis acid sites after desorption at 100 °C and higher, as already suggested. The LAS strength was lower in hybrid materials in comparison to **SiSn-parent** (Table S11). The LAS concentration of **SiSn-parent** was 0.195 mmol g^{-1} (Table 6). A substantial part of acid sites was apparently either blocked by organic moieties or converted to inactive species upon trimethylsilylation. The more trimethylsilyl groups on the surface, the lower the acid site concentration: 0.072 mmol g^{-1} and 0.041 mmol g^{-1} for less and more modified tin silicates, respectively. The specific surface area decreased after modification (Table 5), still the acid site concentration per SA_{BET} (Table S11) drops down. Thus, specific surface area loss is therefore not the only reason for the lower acid site numbers in **SiSn-4Me3Si** and **SiSn-7Me3Si** in comparison to **SiSn-parent**. Steric hindrance of active sites by bulky trimethylsilyl groups (apparently significant as illustrated by the decrease of SA_{micro}, Figure 7 and Table 5, and discussion thereby) can contribute to a decrease of acid site

Table 6. Acidity of Tin Silicates Determined by IR Spectroscopy Combined with Pyridine Adsorption

		Lewis acid sites (mmol g^{-1})			
sample	$^{c}_{Sn,ICP-OES}$ (mmol g^{-1})	100 °C	150 °C	200 °C	250 °C
SiSn-parent	0.139	0.195	0.117	0.044	0.0207
SiSn-4Me3Si	0.132	0.072	0.034	0.012	0.005
SiSn-7Me3Si	0.131	0.041	0.020	0.010	0

https://doi.org/10.1021/acscatal.6c00144
ACS Catal. 2026, 16, 8199−8217

numbers. Last but not least, some tin sites could have been deactivated via coordination of trimethyl(methoxy)silane or methanol (silylation precursor and product, respectively). Methoxy groups were observed in modified materials via ^{13}C MAS NMR and IR spectroscopy (Figure S12C and Figure 9B,C below).

Further insight was gained into the acidity and surface Si−OH groups (Figure S16) by probing the samples with acetonitrile-d_3 (Figure 10). CD_3CN interacted with various species spanning from 2350 to 2250 cm^{-1} whose individual components were further deconvoluted. An example of deconvolution, taking all species (open sites, closed sites, speculative $Sn(OH)_2$, SiOH, gas phase CD_3CN) into account, is provided in Figure S17. The 3800−3200 cm^{-1} region evolved owing to interactions of OH groups with CD_3CN (Figures S18A,B and S19A,B, and S20A,B). Several trends consistent with IR-py analysis can be identified. First, hydrogen bonded SiOH groups gave rise to a positive broad band in the range of 3600−3200 cm^{-1} upon CD_3CN adsorption. Their intensity gradually dropped with desorption time. In parallel, the most pronounced decrease in the CD_3CN range with desorption time was observed for the absorption band at 2275 cm^{-1} corresponding to silanol groups (Figures S18C,D and S19C,D, and S20C,D). This phenomenon is consistent with previous observations reported for Sn-Beta zeolite.[57] Second, notable changes in the OH stretching region persisted even after substantial CD_3CN desorption from SiOH groups (2275 cm^{-1}) suggesting an additional CD_3CN interaction with tin-related species (e.g. O_3SnOH, $O_2Sn(OH)_2$) and SiOH located in close proximity to tin sites.

Furthermore, an evident increase in isolated SiOH groups (~3745 cm^{-1}) was observed for both parent and modified samples upon CD_3CN adsorption. Similarly to IR-py analysis, this effect likely arises from the disruption of hydrogen bonding between silanols by CD_3CN adsorption, leading to the formation of isolated groups. Like modified samples after pyridine adsorption, the absorption band at 3735 cm^{-1} was also involved in interaction with CD_3CN as indicated by its negative intensity. As suggested above and elsewhere,[74] this band might be tentatively assigned to geminal groups.

Importantly, the concentration of silanol groups according to the band at 2275 cm^{-1} decreased for the samples after modification (Figure 10 and Table S12). It further supports the already discussed results on the successful ≡Si−OH group conversion to ≡Si−$OSiMe_3$ moieties (XPS, IR, and MAS NMR spectroscopy; see above).

The total acid sites numbers based on Sn assessed via acetonitrile-d_3 adsorption decreased upon trimethylsilylation (Table S12) which agrees with IR-py analysis (Figure S21). The numbers of putative $Sn(OH)_2$ species were very low in all samples. Both open and closed acid site numbers decreased after surface modification. As already discussed, the decrease of both open and closed acid sites (i.e., LAS) upon trimethylsilylation might originate in (i) surface area decrease, (ii) micropore blockage, (iii) steric hindrance of bulky trimethylsilyl groups, and (iv) coordination of trimethyl(methoxy)silane and/or methanol on tin sites. The open to closed acid sites ratio varied around unity without any clear trend upon trimethylsilylation

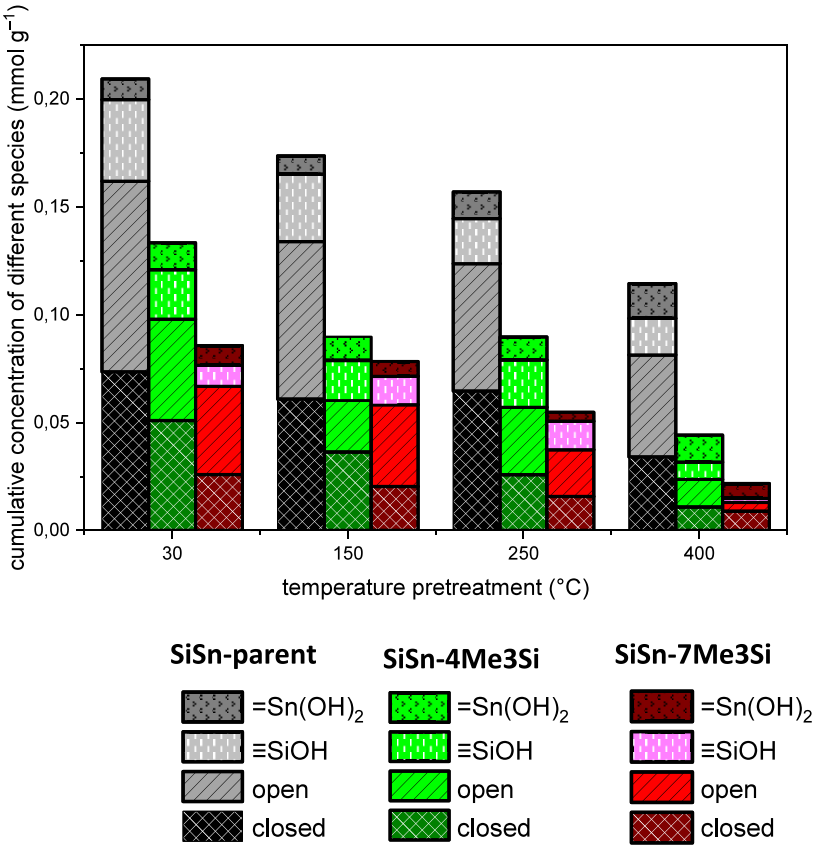

Figure 10. Concentration of open, closed, $Sn(OH)_2$, and SiOH species in (hybrid) tin silicates with different temperature pretreatments determined by IR-CD_3CN.

https://doi.org/10.1021/acscatal.6c00144
ACS Catal. 2026, 16, 8199−8217

(Table S12). Therefore, trimethyl(methoxy)silane appears to block the acid sites nonselectively.

3.2.3. Ethyl Lactate Production over Surface Modified Tin Silicate Catalysts. Pretreated (hybrid) tin silicate catalysts (dried in an oven at 110 °C overnight) were tested in liquid ethanol under reflux for EL production from DHA. The fully inorganic tin silicate (**SiSn-parent**) reached the DHA conversion of 57% after 6 h, which was very similar to the modified samples **SiSn-4Me3Si** and **SiSn-7Me3Si** (Figure 11A). The selectivity to EL over modified catalysts, however, was improved with modified catalysts in comparison to **SiSn-parent** (Figure 11C) similar to results reported by Li et al. (Table S13, XS-Sn-MCM-41-A vs. silylated XS-Sn-MCM-41-A).[12] Thus, EL yield was enhanced over modified samples.

Strikingly, the catalytic activity of SiSn-parent (dried in an oven at 110 °C overnight) did not reach the DHA conversion reported in the first part of the study (vide supra, analogic sample SiSn-RCl+Ac, exposed to air overnight). Therefore, we tried to test the SiSn-parent under similar conditions, i.e., exposed to air overnight. It resulted in obtaining reproducible results; DHA conversion reached 73% and 79% over SiSn-parent and SiSn-RCl+Ac, respectively. Therefore, modified catalysts were tested again after exposure to air and, interestingly, provided different results (Figure 11A, C vs. 11B,D). The DHA conversion and selectivity to EL over SiSn-7Me3Si remained very close to the dry samples, but it improved for SiSn-4Me3Si and, to a higher extent, for SiSn-parent. Thus, the DHA conversion and the selectivity towards EL over air exposed (wet) samples decreased more significantly as a higher number of trimethylsilyl groups was attached to the surface. In the first part of the study, the DHA conversion and EL selectivity correlated well with the LAS numbers. It was evidenced by a similar $TOF_{EL,LAS,100}$ observed for **SiSn-Ac** and **SiSn-RCl+Ac** (see Section 3.1.2 in the main text and 3.1.4 and 3.1.5 in Supporting Information). This possible explanation of different catalytic activities of **SiSn-parent**, **SiSn-4Me3Si**, and **SiSn-7Me3Si** (i.e., the scaling of catalytic activity with acid site numbers), however, fails in the case of modified samples studied herein (Figure 12). The turnover frequency in both dry and wet catalysts shows a significant improvement upon trimethylsilylation: Apparent turnover

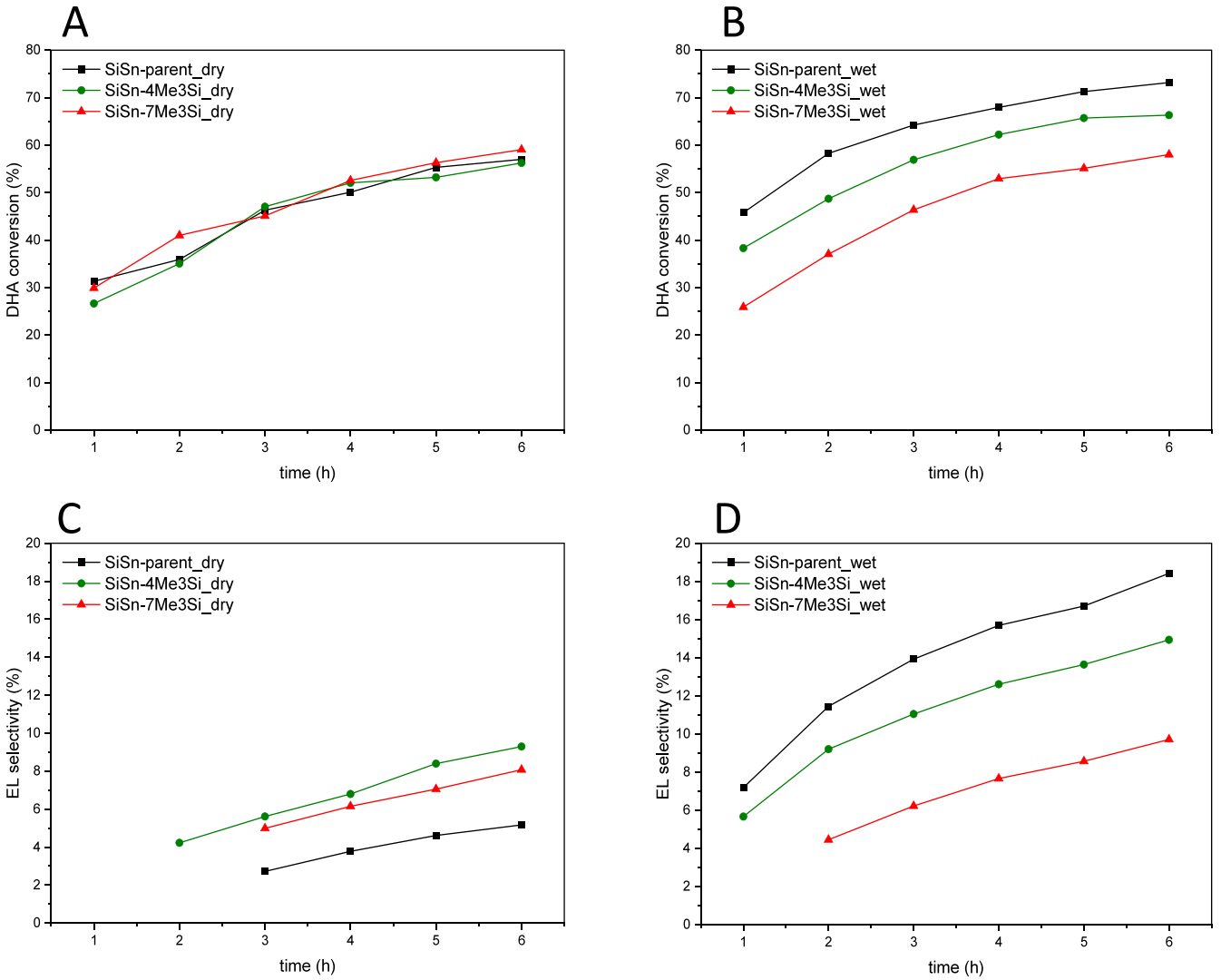

Figure 11. Dihydroxyacetone conversion (A, B) and selectivity to ethyl lactate (C, D) over pretreated (A, C) and nontreated (B, D) tin silicate catalysts.

https://doi.org/10.1021/acscatal.6c00144
ACS Catal. 2026, 16, 8199−8217

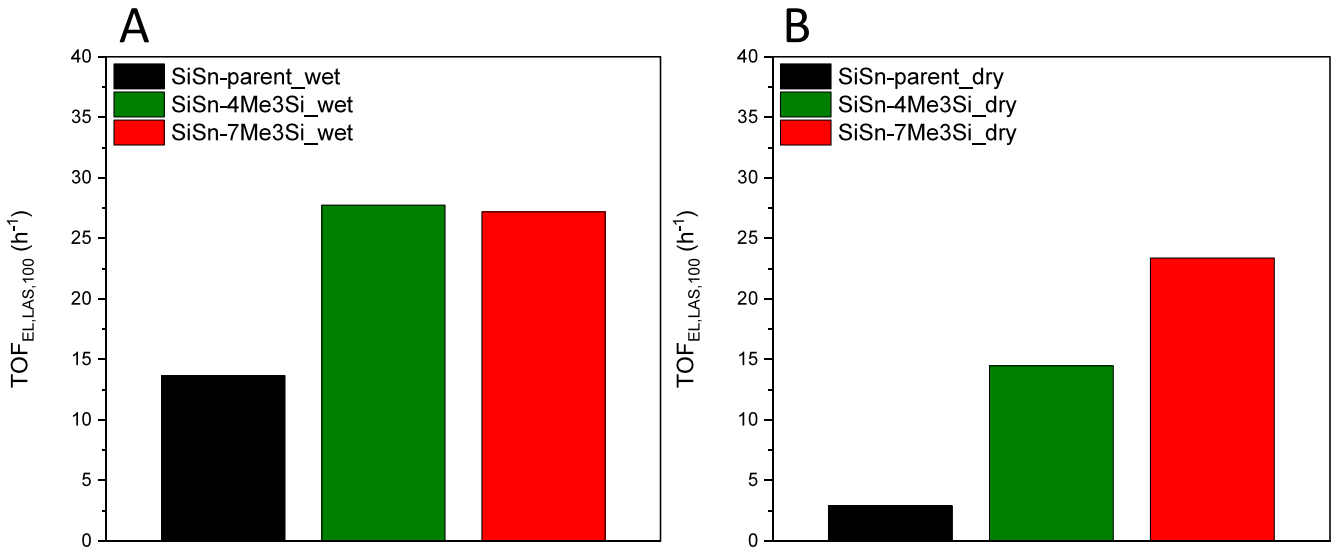

Figure 12. Turnover frequency in ethyl lactate production for air-exposed (A) and temperature pretreated (B) tin silicates after 6 h of reaction, TOF based on Lewis acid site numbers estimated by pyridine adsorption combined with IR spectroscopy (pyridine desorption at 100 °C).

frequency ($TOF_{EL,LAS,100}$) of wet **SiSn-parent** reached 14 mol_{EL} $mol_{acid\ site}^{-1}$ h^{-1}, while $TOF_{EL,LAS,100}$ increased ca. two times for both wet modified samples (Figure 12A). An even clearer trend was observed for pretreated (dry) samples (Figure 12B): the higher the trimethylsilylation degree, the higher the $TOF_{EL,LAS,100}$.

As the catalytic activity in modified tin silicates did not follow the Lewis acid site numbers, it was hypothesized that it might rely on the changing open/closed acid site ratio upon heating and upon trimethylsilylation. Open acid sites have been converted to closed acid sites in Sn-Beta zeolite at 400 °C according to ^{119}Sn MAS NMR.[95] The process was reversible − closed acid sites were transformed back to open sites upon exposure to air for several months.[95] CD_3CN adsorption did not show a similar trend in amorphous tin silicates prepared herein by NHSG (Figure 10 and Table S12). The open/closed acid site ratio varies without any clear trend upon heating and upon trimethylsilylation. Thus, the results in hand do not allow to confirm any hypothesis on the role of open and closed acid sites in EL production although the last step of isomerization was calculated to be more favorable via open sites.[25] An absence of any special role of open and closed acid sites (potentially present but not observed under given conditions) can be further supported by plotting the TOFs over open, closed, and both open and closed acid sites (Figure S22). Importantly, the pattern is similar across all evaluations: The trimethylsilylated samples exhibit a higher TOF than the parent sample (Figure 12 and Figure S22). Thus, open and closed acid sites (IR-CD_3CN) can be assigned to LAS (IR-py; Figure 12 and Figure S22).

Finally, the difference between wet and dry samples in their catalytic performance might be attributed to the number of available silanol groups. The acetonitrile-d_3 adsorption combined with IR spectroscopy showed that the more Me_3Si groups on the surface, the less Si−OH retained in the samples. Moreover, it also showed that higher pretreatment temperatures before acetonitrile-d_3 adsorption provided **the SiSn-parent** sample with significantly lower Si−OH numbers (Figure S16). A higher availability of silanol groups in wet **SiSn-parent** leads to higher catalytic activity. On the contrary, the silanol content only slightly fluctuates in **SiSn-7Me3Si** after evacuation at different temperatures. Thus, dry and wet **SiSn-7Me3Si** exhibit comparable catalytic activity (DHA conversion reached 59% and 58% after 6 h, respectively). As a result, both DHA conversion and EL selectivity follow the order **SiSn-parent > SiSn-4Me3Si > SiSn-7Me3Si** in wet samples due to a different number of Si−OH moieties. Importantly, silanol groups in close proximity to tin atoms (weak Brønsted acid sites) have already been identified as a key factor of highly active catalysts in EL production as they can catalyze the initial step consisting of DHA dehydration but can also promote formation of side products (hemiacetal and acetal).[12]

It appears that, on one hand, trimethylsilylation improves the TOF of tin silicate catalysts. This pronounced activity amplification can be caused by repulsion between hydrophobic trimethylsilyl groups (as determined by WCA) attached to the surface and water resulting from the first step of EL production—DHA dehydration. A positive effect of hydrophobicity on catalytic performance has already been reported for SO aminolysis over aluminosilicates[66], olefin epoxidation over titanosilicates,[21,96,97] or acetophenone hydrogenation over Ni-MCM-41.[98] On the other hand, the trimethylsilylation effectively converts the silanol groups and their contribution to the catalytic activity diminishes. Therefore, a high content of LAS, but a balanced ratio of trimethylsilyl (or methylsilyl[29]) and silanol groups are necessary to achieve high DHA conversions and EL selectivity.

3.2.4. Styrene Oxide Aminolysis over Surface Modified Tin Silicate Catalysts. SO aminolysis was performed over dry and wet SiSn-parent, SiSn-4Me3Si, and SiSn-7Me3Si catalysts. The selectivity to 2-phenyl-2-(phenylamino)ethanol (product I) evaluated at iso-conversion remained similar after trimethylsilyl group attachment for both dry and air exposed samples (Table S14). However, the catalytic activity exhibited the opposite behavior in comparison to EL production: Dry catalysts were ca. twice more active than air exposed materials (Figure 13). SiSn-4Me3Si exhibited the highest catalytic activity in both dry and wet conditions. For example, SO

https://doi.org/10.1021/acscatal.6c00144
ACS Catal. 2026, 16, 8199−8217

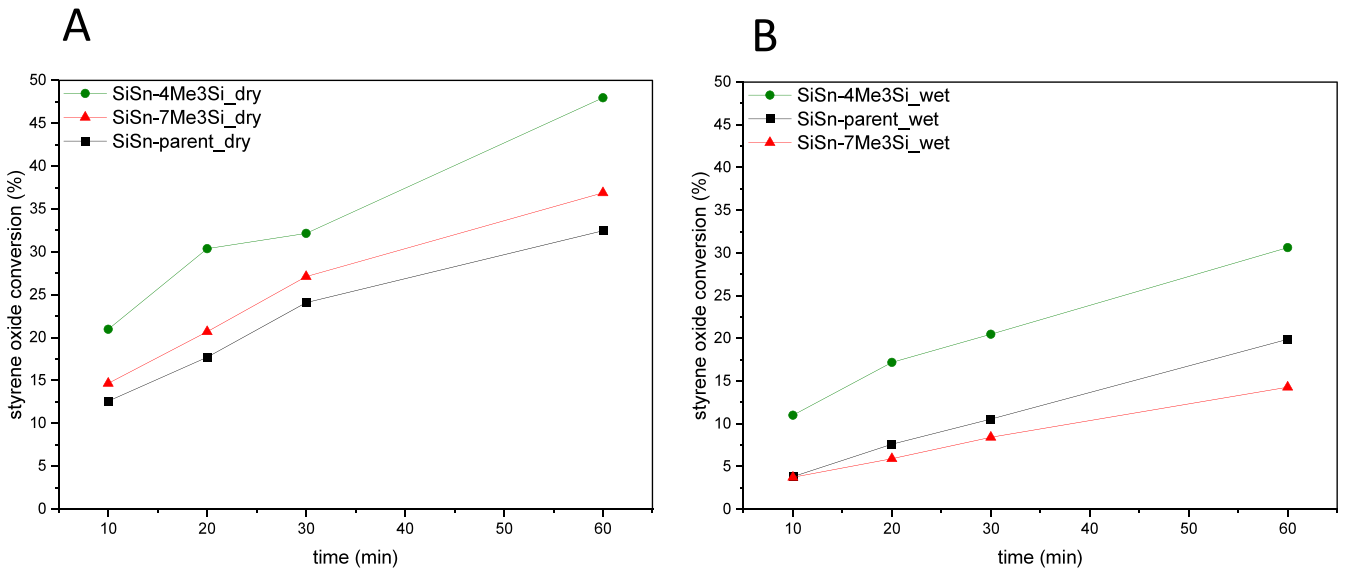

Figure 13. Styrene oxide conversion over temperature pretreated (A) and air-exposed (B) catalysts.

conversion reached almost 50% after 60 min over dry SiSn-4Me3Si. Comparable conversion was obtained over mesoporous SnO2-SiO2 catalysts with significantly higher tin loadings prepared by nonhydrolytic sol-gel at ambient pressure (Table S15).[38]

An apparent turnover frequency, i.e., SO converted per acid site per hour (based on acid site numbers evaluated by pyridine adsorption combined with IR spectroscopy, $TOF_{SO,LAS,100}$) significantly varied (Figure 14). Pristine tin silicate **SiSn-parent** reached a $TOF_{SO,LAS,100}$ of 175 h^{-1}. When a tin silicate was covered by hydrophobic trimethylsilyl groups (as determined by WCA), the $TOF_{SO,LAS,100}$ markedly increased by ca. 4 times for **SiSn-4Me3Si** (770 h^{-1}) and 5 times for **SiSn-7Me3Si** (872 h^{-1}). Similar remarkable improvement has been observed for trimethylsilylated aluminosilicates in styrene oxide aminolysis (from 135 h^{-1} to 705 h^{-1} for parent and highly trimethylsilylated sample, respectively). Kinetic studies performed on aluminosilicates showed that the apparent activation energy increased upon surface modification. The decisive role in catalytic activity improvement was, however, played by the frequency factor that increased by several orders of magnitude upon trimethylsilylation.[66] Noteworthy, the TOF numbers for aluminosilicates and tin silicates reported herein could not be compared directly. The tin silicates were more active although their performance was studied in a higher dilution (Table S15).[66]

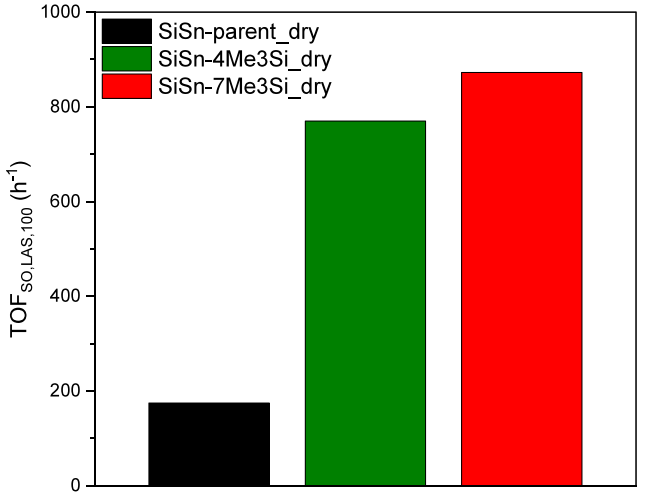

Figure 14. Turnover frequency for temperature pretreated tin silicate and modified samples during aminolysis of styrene oxide (TOF expressed as mol of converted styrene oxide per mol of Lewis acid sites per hour).

The surface modification of tin silicates with trimethyl (methoxy)silane is thus unambiguously beneficial for styrene oxide aminolysis. Hydrophobic trimethylsilyl groups on the surface together with the dry conditions facilitate the conversion of nonpolar styrene oxide and aniline. Exposure to moisture is not desired. This result is in a striking contrast to DHA to EL conversion over the same catalysts.

4. CONCLUSIONS

Tin silicates synthesis has been explored by a nonhydrolytic sol-gel method using three condensation reactions − alkyl halide elimination, acetamide elimination, and alkyl halide elimination combined with delayed acetamide eliminations. The latter route provided porous materials without use of any pore generating agent with high Sn surface concentration and highly homogeneous Sn dispersion in silica. These materials show high activity in the conversion of dihydroxyacetone to ethyl lactate and in the styrene oxide aminolysis reaction. The catalytic activity appears to strongly correlate with Lewis acid site numbers.

Much deeper insight into catalytic performance was gained thanks to the conversion of SiOH groups to $SiOSiMe_3$ moieties via surface modification. This treatment introduced hydrophobic groups on the surface and led to a decrease of acid site numbers. However, their nature (i.e., Lewis acidity, open/closed acid site ratio) has virtually not changed.

Upon trimethylsilyl groups grafting, the turnover frequency increased twice in the DHA to EL reaction and up to 5 times

https://doi.org/10.1021/acscatal.6c00144
ACS Catal. 2026, 16, 8199−8217

in styrene oxide aminolysis. On the one hand, the introduction of hydrophobic trimethylsilyl groups had an unambiguously beneficial impact on the activity in SO conversion. On the other hand, the role of SiOH groups in DHA conversion has been identified. Thus, a balanced SiOH to $SiOSiMe_3$ groups ratio with a high content of Lewis tin acid sites needs to be found to achieve high DHA conversions and EL selectivity.

This work encourages a broader application of NHSG-prepared tin silicates and highlights surface modification as a powerful strategy for unlocking their full catalytic potential and for getting a deeper understanding of the role of surface groups in heterogeneous catalysis.

■ ASSOCIATED CONTENT

Supporting Information

The Supporting Information is available free of charge at https://pubs.acs.org/doi/10.1021/acscatal.6c00144.

General procedures, chemicals, and instrumentation; Characterization of inorganic tin silicates (DR UV−vis spectra, XPS deconvolution data, pore size distribution; acidity characterization via pyridine and CD_3CN adsorption and subsequent IR spectroscopy); catalytic activity of inorganic tin silicates; Characterization of hybrid tin silicates (IR spectra of OH region, XPS spectra, ^{13}C CPMAS NMR spectra, TG analysis, DR UV−vis spectra, acidity characterization via pyridine and CD_3CN adsorption and subsequent IR spectroscopy); Catalytic activity of hybrid tin silicates (PDF)

■ AUTHOR INFORMATION

Corresponding Authors

Damien P. Debecker – *Institute of Condensed Matter and Nanoscience (IMCN), UCLouvain, Place Louis Pasteur 1, Louvain-La-Neuve 1348, Belgium;* orcid.org/0000-0001-6500-2996; Email: damien.debecker@uclouvain.be

Ales Styskalik – *Department of Chemistry, Faculty of Science, Masaryk University, Kotlarska 267/2, Brno CZ-611 37, Czech Republic;* orcid.org/0000-0002-9998-6978; Email: styskalik@chemi.muni.cz

Authors

Lucie Leonova – *Department of Chemistry, Faculty of Science, Masaryk University, Kotlarska 267/2, Brno CZ-611 37, Czech Republic;* orcid.org/0000-0002-8002-8307

Zdenek Moravec – *Department of Chemistry, Faculty of Science, Masaryk University, Kotlarska 267/2, Brno CZ-611 37, Czech Republic;* orcid.org/0000-0003-4377-3575

Petr Sazama – *J. Heyrovsky Institute of Physical Chemistry, Czech Academy of Sciences, Dolejskova 3, Prague 8 CZ-182 23, Czech Republic;* orcid.org/0000-0001-7795-2681

Tomas Pokorny – *Department of Chemistry, Faculty of Science, Masaryk University, Kotlarska 267/2, Brno CZ-611 37, Czech Republic;* orcid.org/0000-0002-6780-4738

Dalibor Kaucky – *J. Heyrovsky Institute of Physical Chemistry, Czech Academy of Sciences, Dolejskova 3, Prague 8 CZ-182 23, Czech Republic*

Areej Fatima – *Department of Plasma Physics and Technology, Faculty of Science, Masaryk University, Kotlarska 267/2, Brno CZ-611 37, Czech Republic*

Tomas Homola – *Department of Plasma Physics and Technology, Faculty of Science, Masaryk University, Kotlarska 267/2, Brno CZ-611 37, Czech Republic;* orcid.org/0000-0002-8522-6169

Complete contact information is available at: https://pubs.acs.org/doi/10.1021/acscatal.6c00144

Notes

The authors declare no competing financial interest.

■ ACKNOWLEDGMENTS

The authors thank L. Simonikova for performing ICP-OES analyses and Zuzana Hlavenkova for STEM-EDS. The primary funding of this work was provided by the project Quantum materials for applications in sustainable technologies (QM4ST), CZ.02.01.01/00/22_008/0004572 by Program Johannes Amos Commenius, call Excellent Research. We acknowledge CF NMR and CryoEM of CIISB, Instruct-CZ Centre, supported by MEYS CR (LM2023042) and European Regional Development Fund-Project "Innovation of Czech Infrastructure for Integrative Structural Biology" (No. CZ.02.01.01/00/23_015/0008175). F.R.S.-FNRS is thanked for covering part of lab expenses of this research via CRD projects FNRS J.0044.20 and FNRS J.0042.25. We also acknowledge the support provided by the Research Infrastructure NanoEnviCz (Projects No. LM2023066, EF18_046/0015586), funded by the Ministry of Education, Youth and Sports of the Czech Republic. CzechNanoLab project LM2023051 funded by MEYS CR is gratefully acknowledged for the financial support of the XPS measurements at CEITEC Nano Research Infrastructure.

■ REFERENCES

(1) Gong, J.; Hao, A.; Liu, W.; Zhan, E.; Shen, W. Efficient Construction of Framework Sn Sites over SnBeta Nanocrystals for Selective Oxidation. *J. Phys. Chem. C* **2025**, *129* (23), 10498–10506.

(2) Li, P.; Liu, G.; Wu, H.; Liu, Y.; Jiang, J. G.; Wu, P. Postsynthesis and Selective Oxidation Properties of Nanosized Sn-Beta Zeolite. *J. Phys. Chem. C* **2011**, *115* (9), 3663–3670.

(3) Palai, Y. N.; Shrotri, A.; Fukuoka, A. Selective Oxidation of Furfural to Succinic Acid over Lewis Acidic Sn-Beta. *ACS Catal.* **2022**, *12* (6), 3534–3542.

(4) Samanta, S.; Mal, N. K.; Manna, A.; Bhaumik, A. Mesoporous Tin Silicate: An Efficient Liquid Phase Oxidative Dehydrogenation Catalyst. *Appl. Catal. A Gen.* **2004**, *273* (1−2), 157–161.

(5) Yue, Y.; Fu, J.; Wang, C.; Yuan, P.; Bao, X.; Xie, Z.; Basset, J. M.; Zhu, H. Propane Dehydrogenation Catalyzed by Single Lewis Acid Site in Sn-Beta Zeolite. *J. Catal.* **2021**, *395*, 155–167.

(6) Vega-Vila, J. C.; Harris, J. W.; Gounder, R. Controlled Insertion of Tin Atoms into Zeolite Framework Vacancies and Consequences for Glucose Isomerization Catalysis. *J. Catal.* **2016**, *344*, 108–120.

(7) Dijkmans, J.; Gabriëls, D.; Dusselier, M.; de Clippel, F.; Vanelderen, P.; Houthoofd, K.; Malfliet, A.; Pontikes, Y.; Sels, B. F. Productive Sugar Isomerization with Highly Active Sn in Dealuminated β Zeolites. *Green Chem.* **2013**, *15* (10), 2777.

(8) Gounder, R.; Davis, M. E. Monosaccharide and Disaccharide Isomerization over Lewis Acid Sites in Hydrophobic and Hydrophilic Molecular Sieves. *J. Catal.* **2013**, *308*, 176–188.

(9) Bermejo-Deval, R.; Orazov, M.; Gounder, R.; Hwang, S. J.; Davis, M. E. Active Sites in Sn-Beta for Glucose Isomerization to Fructose and Epimerization to Mannose. *ACS Catal.* **2014**, *4* (7), 2288–2297.

(10) Boronat, M.; Concepción, P.; Corma, A.; Navarro, M. T.; Renz, M.; Valencia, S. Reactivity in the Confined Spaces of Zeolites: The Interplay

https://doi.org/10.1021/acscatal.6c00144
ACS Catal. 2026, 16, 8199–8217

between Spectroscopy and Theory to Develop Structure−Activity Relationships for Catalysis. *Phys. Chem. Chem. Phys.* **2009**, *11* (16), 2876.
(11) Ford, L.; Spanos, A.; Brunelli, N. A. Counting Sites in Lewis Acid Zeolite Sn-Beta: Connecting Site Quantification Experiments and Spectroscopy To Investigate the Catalytic Activity for the Alcohol Ring Opening of Epoxides. *ACS Catal.* **2023**, *13* (17), 11422–11432.
(12) Li, L.; Collard, X.; Bertrand, A.; Sels, B. F.; Pescarmona, P. P.; Aprile, C. Extra-Small Porous Sn-Silicate Nanoparticles as Catalysts for the Synthesis of Lactates. *J. Catal.* **2014**, *314*, 56–65.
(13) Li, L.; Stroobants, C.; Lin, K.; Jacobs, P. A.; Sels, B. F.; Pescarmona, P. P. Selective Conversion of Trioses to Lactates over Lewis Acid Heterogeneous Catalysts. *Green Chem.* **2011**, *13* (5), 1175.
(14) Van der erren, M.; Corrias, A.; Vykoukal, V.; Styskalik, A.; Aprile, C.; Debecker, D. P. Bifunctional Au−Sn-SiO 2 Catalysts Promote the Direct Upgrading of Glycerol to Methyl Lactate. *Nanoscale* **2024**, *16* (16), 7988–8001.
(15) Dijkmans, J.; Dusselier, M.; Gabriëls, D.; Houthoofd, K.; Magusin, P. C.; Huang, S.; Pontikes, Y.; Trekels, M.; Vantomme, A.; Giebeler, L.; et al. Cooperative Catalysis for Multistep Biomass Conversion with Sn/Al Beta Zeolite. *ACS Catal.* **2015**, *5* (2), 928–940.
(16) de Clippel, F.; Dusselier, M.; Van Rompaey, R.; Vanelderen, P.; Dijkmans, J.; Makshina, E.; Giebeler, L.; Oswald, S.; Baron, G. V.; Denayer, J. F.; et al. Fast and Selective Sugar Conversion to Alkyl Lactate and Lactic Acid with Bifunctional Carbon−Silica Catalysts. *J. Am. Chem. Soc.* **2012**, *134* (24), 10089–10101.
(17) Wolf, P.; Liao, W.; Ong, T. C.; Valla, M.; Harris, J. W.; Gounder, R.; van der Graaff, W. N.; Pidko, E. A.; Hensen, E. J.; Ferrini, P.; et al. Identifying Sn Site Heterogeneities Prevalent Among Sn−Beta Zeolites. *Helv. Chim. Acta* **2016**, *99* (12), 916–927.
(18) Harris, J. W.; Liao, W. C.; Di Iorio, J. R.; Henry, A. M.; Ong, T. C.; Comas-Vives, A.; Copéret, C.; Gounder, R. Molecular Structure and Confining Environment of Sn Sites in Single-Site Chabazite Zeolites. *Chem. Mater.* **2017**, *29* (20), 8824–8837.
(19) Rajalakshmi, R.; Srinivasan, V. V.; Pachamuthu, M. P.; Maheswari, R. Characterizations of Tin (SnO2) Doped KIT-5 by Direct Synthesis. *Mater. Chem. Phys.* **2015**, *154*, 164–169.
(20) Dai, W.; Lei, Q.; Wu, G.; Guan, N.; Hunger, M.; Li, L. Spectroscopic Signature of Lewis Acidic Framework and Extraframework Sn Sites in Beta Zeolites. *ACS Catal.* **2020**, *10* (23), 14135–14146.
(21) Silvestre-Alberó, J.; Domine, M. E.; Jordá, J. L.; Navarro, M. T.; Rey, F.; Rodríguez-Reinoso, F.; Corma, A. Spectroscopic, Calorimetric, and Catalytic Evidences of Hydrophobicity on Ti-MCM-41 Silylated Materials for Olefin Epoxidations. *Appl. Catal. A Gen.* **2015**, *507*, 14–25.
(22) Peeters, E.; Pomalaza, G.; Khalil, I.; Detaille, A.; Debecker, D. P.; Douvalis, A. P.; Dusselier, M.; Sels, B. F. Highly Dispersed Sn-Beta Zeolites as Active Catalysts for Baeyer−Villiger Oxidation: The Role of Mobile, In Situ Sn(II)O Species in Solid-State Stannation. *ACS Catal.* **2021**, *11* (10), 5984–5998.
(23) Boronat, M.; Concepcion, P.; Corma, A.; Renz, M.; Valencia, S. Determination of the Catalytically Active Oxidation Lewis Acid Sites in Sn-Beta Zeolites, and Their Optimisation by the Combination of Theoretical and Experimental Studies. *J. Catal.* **2005**, *234* (1), 111–118.
(24) Boronat, M.; Corma, A.; Renz, M. Mechanism of the Meerwein−Ponndorf−Verley−Oppenauer (MPVO) Redox Equilibrium on Sn− and Zr−Beta Zeolite Catalysts. *J. Phys. Chem. B* **2006**, *110* (42), 21168–21174.
(25) van der Graaff, W. N.; Li, G.; Mezari, B.; Pidko, E. A.; Hensen, E. J. M. Synthesis of Sn−Beta with Exclusive and High Framework Sn Content. *ChemCatChem* **2015**, *7* (7), 1152–1160.
(26) Bates, J. S.; Gounder, R. Influence of Confining Environment Polarity on Ethanol Dehydration Catalysis by Lewis Acid Zeolites. *J. Catal.* **2018**, *365*, 213–226.
(27) Di Iorio, J. R.; Johnson, B. A.; Román-Leshkov, Y. Ordered Hydrogen-Bonded Alcohol Networks Confined in Lewis Acid Zeolites Accelerate Transfer Hydrogenation Turnover Rates. *J. Am. Chem. Soc.* **2020**, *142* (45), 19379–19392.
(28) Zhang, J.; Bo, S.; Liao, W.; Yang, K.; Su, T.; Lü, H.; Zhu, Z. Pore-Engineering-Dependence and Hydrophobicity-Dependence on Stannosilicate Zeolite Catalyst for Efficient Baeyer-Villiger Oxidation. *Fuel* **2024**, *357*, No. 129662 .
(29) Vivian, A.; Fusaro, L.; Debecker, D. P.; Aprile, C. Mesoporous Methyl-Functionalized Sn-Silicates Generated by the Aerosol Process for the Sustainable Production of Ethyl Lactate. *ACS Sustain. Chem. Eng.* **2018**, *6* (11), 14095–14103.
(30) Spanos, A. P.; Parulkar, A.; Brunelli, N. A. Enhancing Hydrophobicity and Catalytic Activity of Nano-Sn-Beta for Alcohol Ring Opening of Epoxides through Post-Synthetic Treatment with Fluoride. *J. Catal.* **2021**, *404*, 430–439.
(31) Hammond, C.; Padovan, D.; Al−Nayili, A.; Wells, P. P.; Gibson, E. K.; Dimitratos, N. Identification of Active and Spectator Sn Sites in Sn−β Following Solid−State Stannation, and Consequences for Lewis Acid Catalysis. *ChemCatChem* **2015**, *7* (20), 3322–3331.
(32) Wolf, P.; Hammond, C.; Conrad, S.; Hermans, I. Post-Synthetic Preparation of Sn-, Ti- and Zr-Beta: A Facile Route to Water Tolerant, Highly Active Lewis Acidic Zeolites. *Dalton Trans.* **2014**, *43* (11), 4514.
(33) Ivanushkin, G.; Torka Beydokhti, M.; Martinez-Espin, J. S.; Dusselier, M. Electro-Assisted Synthesis of Sn-Beta Zeolite Leads to Record Tin Incorporation and Superior Lewis Acid Catalysis. *Chem. Mater.* **2023**, *35* (23), 10216–10227.
(34) Zhu, J.; Tay, B. Y.; Ma, J. Hydrothermal Synthesis and Characterization of Mesoporous SnO2/SnO2−SiO2 on Neutral Template. *J. Mater. Process. Technol.* **2007**, *192*, 61–566.
(35) Godard, N.; Vivian, A.; Fusaro, L.; Cannavicci, L.; Aprile, C.; Debecker, D. P. High-Yield Synthesis of Ethyl Lactate with Mesoporous Tin Silicate Catalysts Prepared by an Aerosol-Assisted Sol-Gel Process. *ChemCatChem* **2017**, *9* (12), 2211–2218.
(36) Gopalakrishnan, M.; Palanisami, N. New sterically hindered tin (IV) siloxane precursors to tinsilicate materials: synthesis, spectral, structural and photocatalytic studies. *RSC Adv.* **2016**, *6* (3), 1760–1768.
(37) Kirszensztejn, P.; Kawałko, A.; Tolińska, A.; Przekop, R. Synthesis of SiO2−SnO2 Gels in Water Free Conditions. *J. Porous Mater.* **2011**, *18* (2), 241–249.
(38) Skoda, D.; Styskalik, A.; Moravec, Z.; Bezdicka, P.; Bursik, J.; Mutin, P. H.; Pinkas, J. Mesoporous SnO_2-SiO_2 and Sn-Silica-Carbon Nanocomposites by Novel Non-Hydrolytic Templated Sol-Gel Synthesis. *RSC Adv.* **2016**, *6* (73), 68739–68747.
(39) Leonhardt, C.; Brumm, S.; Seifert, A.; Cox, G.; Lange, A.; Rüffer, T.; Schaarschmidt, D.; Lang, H.; Jöhrmann, N.; Hietschold, M.; et al. Tin Oxide Nanoparticles and SnO_2 /SiO_2 Hybrid Materials by Twin Polymerization Using Tin(IV) Alkoxides. *ChemPlusChem* **2013**, *78* (11), 1400–1412.
(40) Styskalik, A.; Vykoukal, V.; Fusaro, L.; Aprile, C.; Debecker, D. P. Mildly Acidic Aluminosilicate Catalysts for Stable Performance in Ethanol Dehydration. *Appl. Catal., B* **2020**, *271*, No. 118926 .
(41) Dochain, D. D.; Styskalik, A.; Vykoukal, V.; Vimont, A.; Travert, A.; Debecker, D. P. Non-Hydrolytic Sol−Gel Routes to Bifunctional Cu−Ta−SiO_2 Catalysts for the Upgrading of Ethanol to Butadiene. *Chem. Mater.* **2023**, *35* (17), 7113–7124.
(42) Debecker, D. P.; Bouchmella, K.; Delaigle, R.; Eloy, P.; Poleunis, C.; Bertrand, P.; Gaigneaux, E. M.; Mutin, P. H. One-Step Non-Hydrolytic Sol−Gel Preparation of Efficient V_2O_5-TiO_2 Catalysts for VOC Total Oxidation. *Appl. Catal., B* **2010**, *94* (1−2), 38–45.
(43) Skoda, D.; Styskalik, A.; Moravec, Z.; Bezdicka, P.; Babiak, M.; Klementova, M.; Barnes, C. E.; Pinkas, J. Novel Non-Hydrolytic Templated Sol−Gel Synthesis of Mesoporous Aluminosilicates and Their Use as Aminolysis Catalysts. *RSC Adv.* **2016**, *6* (29), 24273–24284.
(44) Skoda, D.; Styskalik, A.; Moravec, Z.; Bezdicka, P.; Barnes, C. E.; Pinkas, J. Mesoporous Titanosilicates by Templated Non-Hydrolytic Sol−Gel Reactions. *J. Sol-Gel Sci. Technol.* **2015**, *74* (3), 810–822.
(45) Lorret, O.; Lafond, V.; Mutin, P. H.; Vioux, A. One-Step Synthesis of Mesoporous Hybrid Titania−Silica Xerogels for the Epoxidation of Alkenes. *Chem. Mater.* **2006**, *18* (20), 4707–4709.
(46) Debecker, D. P.; Bouchmella, K.; Poleunis, C.; Eloy, P.; Bertrand, P.; Gaigneaux, E. M.; Mutin, P. H. Design of SiO_2 −Al_2O_3 −MoO_3

https://doi.org/10.1021/acscatal.6c00144
ACS Catal. 2026, 16, 8199−8217

Metathesis Catalysts by Nonhydrolytic Sol−Gel. *Chem. Mater.* **2009**, *21* (13), 2817–2824.
(47) Lafond, V.; Mutin, P. H.; Vioux, A. Non-Hydrolytic Sol−Gel Routes Based on Alkyl Halide Elimination: Toward Better Mixed Oxide Catalysts and New Supports. *J. Mol. Catal. A Chem.* **2002**, *182−183*, 81–88.
(48) Lafond, V.; Mutin, P. H.; Vioux, A. Control of the Texture of Titania−Silica Mixed Oxides Prepared by Nonhydrolytic Sol−Gel. *Chem. Mater.* **2004**, *16* (25), 5380–5386.
(49) Andrianainarivelo, M.; Corriu, R.; Leclercq, D.; Mutin, P. H.; Vioux, A. Mixed Oxides SiO2−ZrO2 and SiO2−TiO2 by a Non-Hydrolytic Sol−Gel Route. *J. Mater. Chem.* **1996**, *6* (10), 1665–1671.
(50) Mutin, P. H.; Vioux, A. Nonhydrolytic Processing of Oxide-Based Materials: Simple Routes to Control Homogeneity, Morphology, and Nanostructure. *Chem. Mater.* **2009**, *21* (4), 582–596.
(51) Styskalik, A.; Skoda, D.; Barnes, C.; Pinkas, J. The Power of Non-Hydrolytic Sol-Gel Chemistry: A Review. *Catalysts* **2017**, *7* (6), 168.
(52) Smeets, V.; Styskalik, A.; Debecker, D. P. Non-Hydrolytic Sol−Gel as a Versatile Route for the Preparation of Hybrid Heterogeneous Catalysts. *J. Sol-Gel Sci. Technol.* **2021**, *97* (3), 505–522.
(53) Gunther, W. R.; Wang, Y.; Ji, Y.; Michaelis, V. K.; Hunt, S. T.; Griffin, R. G.; Román-Leshkov, Y. Sn-Beta Zeolites with Borate Salts Catalyse the Epimerization of Carbohydrates via an Intramolecular Carbon Shift. *Nat. Commun.* **2012**, *3*, 1109–1116.
(54) Kriesel, J. W.; Sander, M. S.; Tilley, T. D. Block Copolymer-Assisted Synthesis of Mesoporous, Multicomponent Oxides by Nonhydrolytic, Thermolytic Decomposition of Molecular Precursors in Nonpolar Media. *Chem. Mater.* **2001**, *13* (10), 3554–3563.
(55) Skoda, D.; Styskalik, A.; Moravec, Z.; Bezdicka, P.; Pinkas, J. Templated Non-Hydrolytic Synthesis of Mesoporous Zirconium Silicates and Their Catalytic Properties. *J. Mater. Sci.* **2015**, *50* (9), 3371–3382.
(56) Hradsky, D.; Machac, P.; Skoda, D.; Leonova, L.; Sazama, P.; Pastvova, J.; Kaucky, D.; Vsiansky, D.; Moravec, Z.; Styskalik, A. Catalytic Performance of Micro-Mesoporous Zirconosilicates Prepared by Non-Hydrolytic Sol-Gel in Ethanol-Acetaldehyde Conversion to Butadiene and Related Reactions. *Appl. Catal. A Gen.* **2023**, *652*, No. 119037.
(57) Harris, J. W.; Cordon, M. J.; Di Iorio, J R; Vega-Vila, J. C.; Ribeiro, F. H.; Gounder, R. Titration and Quantification of Open and Closed Lewis Acid Sites in Sn-Beta Zeolites That Catalyze Glucose Isomerization. *J. Catal.* **2016**, *335*, 141–154.
(58) Tang, B.; Dai, W.; Wu, G.; Guan, N.; Li, L.; Hunger, M. Improved Postsynthesis Strategy to Sn-Beta Zeolites as Lewis Acid Catalysts for the Ring-Opening Hydration of Epoxides. *ACS Catal.* **2014**, *4* (8), 2801–2810.
(59) Meng, Q.; Liu, J.; Xiong, G.; Liu, X.; Liu, L.; Guo, H. Aerosol-Seed-Assisted Hydrothermal Synthesis of Sn-Beta Zeolite and Its Catalytic Performance in Baeyer−Villiger Oxidation. *Microporous Mesoporous Mater.* **2018**, *266*, 242–251.
(60) Yang, X.; Liu, Y.; Li, X.; Ren, J.; Zhou, L.; Lu, T.; Su, Y. Synthesis of Sn-Containing Nanosized Beta Zeolite As Efficient Catalyst for Transformation of Glucose to Methyl Lactate. *ACS Sustain. Chem. Eng.* **2018**, *6* (7), 8256–8265.
(61) Styskalik, A.; Kordoghli, I.; Poleunis, C.; Delcorte, A.; Moravec, Z.; Simonikova, L.; Kanicky, V.; Aprile, C.; Fusaro, L.; Debecker, D. P. Hybrid Mesoporous Aluminosilicate Catalysts Obtained by Non-Hydrolytic Sol−Gel for Ethanol Dehydration. *J. Mater. Chem. A* **2020**, *8* (44), 23526–23542.
(62) Sun, P.; Liu, C.; Wang, H.; Liao, Y.; Li, X.; Liu, Q.; Sels, B. F.; Wang, C. Rational Positioning of Metal Ions to Stabilize Open Tin Sites in Beta Zeolite for Catalytic Conversion of Sugars. *Angew. Chem., Int. Ed.* **2023**, *62* (6), No. e202215737.
(63) Sushkevich, V. L.; Ivanova, I. I.; Yakimov, A. V. Revisiting Acidity of SnBEA Catalysts by Combined Application of FTIR Spectroscopy of Different Probe Molecules. *J. Phys. Chem. C* **2017**, *121* (21), 11437–11447.
(64) Abidi, N.; Boudjema, Y.; Rivallan, M.; Chizallet, C.; Larmier, K. Challenging the Distinction between "Open" and "Closed" Sn Sites in β Zeolite by Deuterated Acetonitrile Adsorption: Experimental and Theoretical Insights. *J. Phys. Chem. C* **2025**, *129* (31), 14011–14019.
(65) Abidi, N.; Boudjema, Y.; Chizallet, C.; Larmier, K. Investigating Closed and Open Site Stability of Sn-, Ti-, Zr-, and Hf-Beta Zeolites: A Comprehensive Periodic DFT Study. *J. Phys. Chem. C* **2024**, *128* (20), 8257–8269.
(66) Leonova, L.; Moravec, Z.; Sazama, P.; Pastvova, J.; Kobera, L.; Brus, J.; Styskalik, A. Hydrophobicity Boosts Catalytic Activity: The Tailoring of Aluminosilicates with Trimethylsilyl Groups**. *ChemCatChem* **2023**, *15* (13).
(67) Styskalik, A.; Skoda, D.; Pinkas, J.; Mathur, S. Non-Hydrolytic Synthesis of Titanosilicate Xerogels by Acetamide Elimination and Their Use as Epoxidation Catalysts. *J. Sol-Gel Sci. Technol.* **2012**, *63* (3), 463–472.
(68) Corma, A. Water-Resistant Solid Lewis Acid Catalysts: Meerwein−Ponndorf−Verley and Oppenauer Reactions Catalyzed by Tin-Beta Zeolite. *J. Catal.* **2003**, *215* (2), 294–304.
(69) Dapsens, P. Y.; Menart, M. J.; Mondelli, C.; Pérez-Ramírez, J. Production of Bio-Derived Ethyl Lactate on GaUSY Zeolites Prepared by Post-Synthetic Galliation. *Green Chem.* **2014**, *16* (2), 589–593.
(70) Sorriso, S.; Battistini, C.; Macchia, B.; Macchia, F. Three-Membered Rings. Molecular Structure and Conformation of Aryl Substituted Oxiranes by Dipole Moment Measurements. *Z. Naturforsch., B* **1977**, *32* (12), 1467–1472.
(71) Laurence, C.; Nicolet, P.; Dalati, M. T.; Abboud, J. L. M.; Notario, R. The Empirical Treatment of Solvent-Solute Interactions: 15 Years of .Pi. *J. Phys. Chem.* **1994**, *98* (23), 5807–5816.
(72) Morrow, B. A.; McFarlan, A. J. Chemical Reactions at Silica Surfaces. *J. Non-Cryst. Solids* **1990**, *120* (1−3), 61–71.
(73) Prodinger, S.; Derewinski, M. A.; Vjunov, A.; Burton, S. D.; Arslan, I.; Lercher, J. A. Improving Stability of Zeolites in Aqueous Phase via Selective Removal of Structural Defects. *J. Am. Chem. Soc.* **2016**, *138* (13), 4408–4415.
(74) Gallas, J. P.; Goupil, J. M.; Vimont, A.; Lavalley, J. C.; Gil, B.; Gilson, J. P.; Miserque, O. Quantification of Water and Silanol Species on Various Silicas by Coupling IR Spectroscopy and In-Situ Thermogravimetry. *Langmuir* **2009**, *25* (10), 5825–5834.
(75) Janin, A.; Maache, M.; Lavalley, J. C.; Joly, J. F.; Raatz, F.; Szydlowski, N. FT i.r Study of the Silanol Groups in Dealuminated HY Zeolites: Nature of the Extraframework Debris. *Zeolites* **1991**, *11* (4), 391–396.
(76) Omegna, A.; Vasic, M.; Anton van Bokhoven, J.; Pirngruber, G.; Prins, R. Dealumination and Realumination of Microcrystalline Zeolite Beta: An XRD, FTIR and Quantitative Multinuclear (MQ) MAS NMR Study. *Phys. Chem. Chem. Phys.* **2004**, *6* (2), 447.
(77) Zecchina, A.; Bordiga, S.; Spoto, G.; Marchese, L.; Petrini, G.; Leofanti, G.; Padovan, M. Silicalite Characterization. 2. IR Spectroscopy of the Interaction of Carbon Monoxide with Internal and External Hydroxyl Groups. *J. Phys. Chem.* **1992**, *96* (12), 4991–4997.
(78) Dijkmans, J.; Dusselier, M.; Janssens, W.; Trekels, M.; Vantomme, A.; Breynaert, E.; Kirschhock, C.; Sels, B. F. An Inner-/Outer-Sphere Stabilized Sn Active Site in β-Zeolite: Spectroscopic Evidence and Kinetic Consequences. *ACS Catal.* **2016**, *6* (1), 31–46.
(79) Prodinger, S.; Shi, H.; Eckstein, S.; Hu, J. Z.; Olarte, M. V.; Camaioni, D. M.; Derewinski, M. A.; Lercher, J. A. Stability of Zeolites in Aqueous Phase Reactions. *Chem. Mater.* **2017**, *29* (17), 7255–7262.
(80) Lippmaa, E.; Maegi, M.; Samoson, A.; Tarmak, M.; Engelhardt, G. Investigation of the Structure of Zeolites by Solid-State High-Resolution Silicon-29 NMR Spectroscopy. *J. Am. Chem. Soc.* **1981**, *103* (17), 4992–4996.
(81) Toba, M.; Mizukami, F.; Niwa, S. I.; Sano, T.; Maeda, K.; Shoji, H. Effect of Preparation Methods on Properties of Amorphous Alumina/Silicas. *J. Mater. Chem.* **1994**, *4* (7), 1131.
(82) Koyano, K. A.; Tatsumi, T.; Tanaka, Y.; Nakata, S. Stabilization of Mesoporous Molecular Sieves by Trimethylsilylation. *J. Phys. Chem. B.* **1997**, *101* (46), 9436–9440.
(83) Su, D.; Yan, X.; Liu, N.; Li, X.; Ji, H. Preparation and Characterization of Continuous SiZrOC Fibers by Polyvinyl

Pyrrolidone-Assisted Sol−Gel Process. *J. Mater. Sci.* **2016**, *51* (3), 1418–1427.
(84) Guiton, T. A.; Pantano, C. G. Infrared Reflectance Spectroscopy of Porous Silicas. *Colloids Surf. A Physicochem. Eng. Aspects* **1993**, *74* (1), 33–46.
(85) Silva, A. R.; Albuquerque, H.; Borges, S.; Siegel, R.; Mafra, L.; Carvalho, A. P.; Pires, J. Strategies for Copper Bis(Oxazoline) Immobilization onto Porous Silica Based Materials. *Microporous Mesoporous Mater.* **2012**, *158*, 26–38.
(86) Sever, R. R.; Alcala, R.; Dumesic, J. A.; Root, T. W. Vapor-Phase Silylation of MCM-41 and Ti-MCM-41. *Microporous Mesoporous Mater.* **2003**, *66* (1), 53–67.
(87) Olson, D. H.; Haag, W. O.; Borghard, W. S. Use of Water as a Probe of Zeolitic Properties: Interaction of Water with HZSM-5. *Microporous Mesoporous Mater.* **2000**, *35*, 435–446.
(88) Ng, E.-P.; Mintova, S. Nanoporous Materials with Enhanced Hydrophilicity and High Water Sorption Capacity. *Microporous Mesoporous Mater.* **2008**, *114* (1−3), 1–26.
(89) Chaudhari, K.; Das, T. K.; Rajmohanan, P. R.; Lazar, K.; Sivasanker, S.; Chandwadkar, A. J. Synthesis, Characterization, and Catalytic Properties of Mesoporous Tin-Containing Analogs of MCM-41. *J. Catal.* **1999**, *183* (2), 281–291.
(90) Li, L.; Korányi, T. I.; Sels, B. F.; Pescarmona, P. P. Highly-Efficient Conversion of Glycerol to Solketal over Heterogeneous Lewis Acid Catalysts. *Green Chem.* **2012**, *14* (6), No. 1611.
(91) Chakraborty, B.; Viswanathan, B. Surface Acidity of MCM-41 by in Situ IR Studies of Pyridine Adsorption. *Catal. Today* **1999**, *49* (1−3), 253–260.
(92) Turnes Palomino, G.; José Cuart Pascual, J.; Rodrıguez Delgado, M.; Bernardo Parra, J.; Otero Areán, C. FT-IR Studies on the Acidity of Gallium-Substituted Mesoporous MCM-41 Silica. *Mater. Chem. Phys.* **2004**, *85* (1), 145–150.
(93) Topsoe, N. Infrared and Temperature-Programmed Desorption Study of the Acidic Properties of ZSM-5-Type Zeolites. *J. Catal.* **1981**, *70* (1), 41–52.
(94) Sushkevich, V. L.; Kots, P. A.; Kolyagin, Y. G.; Yakimov, A. V.; Marikutsa, A. V.; Ivanova, I. I. Origin of Water-Induced Brønsted Acid Sites in Sn-BEA Zeolites. *J. Phys. Chem. C* **2019**, *123* (9), 5540–5548.
(95) Qi, G.; Wang, Q.; Xu, J.; Wu, Q.; Wang, C.; Zhao, X.; Meng, X.; Xiao, F.; Deng, F. Direct Observation of Tin Sites and Their Reversible Interconversion in Zeolites by Solid-State NMR Spectroscopy. *Commun. Chem.* **2018**, *1* (1), 22.
(96) Smeets, V.; Ben Mustapha, L.; Schnee, J.; Gaigneaux, E. M.; Debecker, D. P. Mesoporous SiO2-TiO2 Epoxidation Catalysts: Tuning Surface Polarity to Improve Performance in the Presence of Water. *Mol. Catal.* **2018**, *452*, 123–128.
(97) Manangon-Perugachi, L. E.; Vivian, A.; Eloy, P.; Debecker, D. P.; Aprile, C.; Gaigneaux, E. M. Hydrophobic Titania-Silica Mixed Oxides for the Catalytic Epoxidation of Cyclooctene. *Catal. Today* **2021**, *363*, 128–136.
(98) Costa, D. C.; Bengoa, J. F.; Marchetti, S. G.; Vetere, V. Impact of the Surface Hydrophobicity/Hydrophilicity Ratio on the Catalytic Properties of Ni Nanoparticles/MCM-41 System Used in the Hydrogenation of Acetophenone. *Catal. Today* **2021**, *372*, 20–26.

https://doi.org/10.1021/acscatal.6c00144
ACS Catal. 2026, 16, 8199−8217